

# Detection of C<sub>2</sub>, CN, and NaID absorption in the AGB remnant of HD 56126 <sup>\*</sup> <sup>\*\*</sup>

Eric J. Bakker<sup>1,2</sup>, L.B.F.M. Waters<sup>3,4</sup>, Henny J.G.L.M. Lamers<sup>2,1</sup>, Norman R. Trams<sup>5</sup>, and Frank L.A. Van der Wolf<sup>1</sup>

<sup>1</sup> Astronomical Institute, University of Utrecht, P.O. Box 80000, NL-3508 TA Utrecht, The Netherlands

<sup>2</sup> SRON Laboratory for Space Research, Sorbonnelaan 2, NL-3584 CA Utrecht, The Netherlands

<sup>3</sup> Astronomical Institute, University of Amsterdam, Kruislaan 403, NL-1098 SJ Amsterdam, The Netherlands

<sup>4</sup> SRON Laboratory for Space Research, P.O. Box 800, NL-9700 AV Groningen, The Netherlands

<sup>5</sup> ESTEC, P.O. Box 299, NL-2200 AG Noordwijk (ZH), The Netherlands

Received January 20 1995, accepted September 1995

**Abstract.** We present the detection of molecular absorption lines in the optical spectrum of the post-AGB star HD 56126. The C<sub>2</sub> Phillips A<sup>1</sup>Π<sub>u</sub> – X<sup>1</sup>Σ<sub>g</sub><sup>+</sup> (1,0), (2,0), and (3,0); Swan d<sup>3</sup>Π<sub>g</sub> – a<sup>3</sup>Π<sub>u</sub> (0,0) and (1,0); and CN Red system A<sup>2</sup>Π – X<sup>2</sup>Σ<sup>+</sup> (1,0), (2,0), (3,0), and (4,0) bands have been identified. From the identification of the molecular bands we find an expansion velocity of  $8.5 \pm 0.6$  km s<sup>-1</sup> independent of excitation condition or molecular specie. On the basis of the expansion velocity, rotational temperatures, and molecular column densities we argue that the line-forming region is the AGB remnant. This is in agreement with the expansion velocity derived from the CO lines. We find column densities of  $\log N_{\text{C}_2} = 15.3 \pm 0.3$  cm<sup>-2</sup> and  $\log N_{\text{CN}} = 15.5 \pm 0.3$  cm<sup>-2</sup>, and rotational temperatures of  $T_{\text{rot}} = 242 \pm 20$  K and  $T_{\text{rot}} = 24 \pm 5$  K respectively for C<sub>2</sub> and CN.

By studying molecular line absorption in optical spectra of post-AGB stars we have found a new tracer of the AGB remnant. From comparison with the results of CO and IR observations it is possible to obtain information on non-spherical behavior of the AGB remnant. Using different molecules with different excitation conditions it should be possible to study the AGB remnant as a function of the distance to the star, and thus as a function of the evolutionary status of the star on the AGB.

**Key words:** line: identification - molecular data - molecular processes - circumstellar matter - stars: individual: HD 56126 - stars: AGB and post-AGB

## 1. Introduction

After the IRAS mission a large number of studies have been conducted in selecting post-Asymptotic Giant Branch (post-AGB) stars based on the IRAS point source catalogue using selection criteria on the infrared colors (e.g., Trams *et al.* 1991; Oudmaijer *et al.* 1992). By looking at the infrared excess one can select sources on its dust geometry (dust density and temperature distribution) rather than on evolutionary status. To be certain about the post-AGB nature one needs additional constraints. HD 56126 not only shows a characteristic infrared excess for post-AGB stars, but also many absorption lines from s-process material. S-process material is only dredged-up to the surface of intermediate-mass stars during the AGB phase (Iben 1983).

During the end of the AGB phase the star suffers from an extreme mass loss rate of typically  $\dot{M}_{\text{AGB}} = 10^{-5} M_{\odot} \text{ yr}^{-1}$ , and the material moves away from the central star with a typical velocity of  $v_{\text{exp}} = 10$  to  $20$  km s<sup>-1</sup>. The dust in the AGB remnant is in radiative equilibrium with the radiation field coming from the star: it absorbs UV and optical radiation and emits the energy in the far-IR. This causes a double-peaked energy distribution, one peak in the optical from the stellar radiation and a second peak in the infrared from the dust shell. The geometry of the mass loss — spherically symmetric or axisymmetric — on the AGB determines the geometry of the dust shell and thus the amount of extinction the central star will suffer as a post-AGB star.

Send offprint requests to: Eric J. Bakker, present address: Astronomy Department, University of Texas, RLM 16.218, Austin, TX 78712, U.S.A., ebakker@astro.as.utexas.edu

\* Based on observations with the Utrecht Echelle Spectrograph on the William Herschel Telescope (La Palma, Spain)

\*\* Tables of App. A are only available in electronic form at the CDS via anonymous ftp 130.79.128.5

HD 56126 has been classified as F5I (Nassau *et al.* 1965) with a strong infrared source peaking at 25  $\mu\text{m}$  (112.8 Jansky; IRAS PSC 1986). In the HD catalogue (published in 1919) HD 56126 is classified as a G5 star, which means that the star has possibly evolved from G5 to F5 in about 50 years.

Knowledge of the mass-loss rate on the AGB and the physical conditions of the AGB remnant are of eminent importance in understanding the AGB and post-AGB evolution of low- and intermediate-mass stars. The amount of mass loss on the AGB seriously affects (i.e., dominates) the mass in the convective envelope of the AGB star. When the envelope mass decreases and reaches a critical value of about  $10^{-2} M_{\odot}$ , the star leaves the AGB and moves along a constant luminosity track to the White Dwarf (WD) phase (Schönberner 1983).

Until now, studies of the AGB remnant of HD 56126 were mainly concentrated on the millimeter and radio line emission of molecules, e.g., <sup>12</sup>CO, <sup>13</sup>CO, HCN (Omont *et al.* 1993), and the tentative detection of HCO<sup>+</sup> (Bujarrabal *et al.* 1992; Nyman *et al.* 1992), as well as the infrared excess (Parthasarathy and Pottasch 1986) and dust features (Kwok *et al.* 1989). Although these are powerful tracers of the AGB remnant, they all face the same problem that these tracers are in emission and that spatial information (projected angle of the velocity vector) and velocity information (expansion velocity) cannot be determined independently if the source is not spatially resolved.

Here we present the detection of molecular absorption lines in the spectrum of the AGB remnant of HD 56126. This allows us to determine outflow velocities, rotational temperatures, column densities, and relative abundances in the AGB remnant at a well-defined position (Bakker *et al.* 1995): in the line of sight to the post-AGB star. Comparison of the results of this work with the results from studies on the emission of the AGB remnant enables us to study the asymmetry of the AGB remnant and mass-loss rates as a function of evolutionary status when the star was still on the AGB.

Here we will first study the optical spectrum of HD 56126. Sect. 2 gives information on how the spectra were obtained and reduced. In Sect. 3 we present the detection of molecular absorption (C<sub>2</sub> and CN) in the AGB remnant. In Sect. 4 we look in detail at the physical conditions of the line-forming region of C<sub>2</sub> and CN, while in Sect. 5 we concentrate on the observed velocities and predict the expected velocities for interstellar lines. We discuss (Sect. 6) these observations in terms of AGB mass loss and evolutionary time scales and summarize the results in Sect. 7. App. A (only available at CDS) gives a line identification list of the molecular lines of the Phillips C<sub>2</sub> (1,0), (2,0), and (3,0) bands and the CN Red system (1,0), (2,0), and (3,0). App. B gives the identification of selected lines of Cl, Ni, and OI.

## 2. Observations and reduction of the echelle spectra

The observations of HD 56126 (Table 1) were made on February 24<sup>th</sup> 1992 by HJGLM using two different grating settings of echelle E31 with the Utrecht Echelle Spectrograph (UES) on the William Herschel Telescope (WHT) on La Palma. The spectra were obtained using the EEV3 detector which has  $1180 \times 1180$   $(\mu\text{m})^2$  pixels. The wavelength coverage of the spectrum is from 4430 to 10302 Å, but inherent to an echelle spectrograph there are wavelength parts in the red ( $\lambda > 6030$  Å) which are not covered by the CCD because the projected echellogram is larger than the size of the CCD detector. The spectra were reduced by Ton Schoenmaker in Roden using the IRAF package: bias subtracted, wavelength calibrated, and continuum corrected. The wavelength calibration was made using a ThAr arc spectrum and a wavelength identification table of 1838 ThAr lines in wavelength range between 3200 and 9548 Å. For wavelengths longer than 9548 Å the wavelength calibration was extrapolated using the fit derived from shorter wavelengths. A log of the spectra is given in Table 2. The velocity resolution was determined from the identified telluric lines (Moore *et al.* 1966). The FWHM spread is  $\approx 1.0 \text{ km s}^{-1}$ . At H $\alpha$  (6563 Å) the signal-to-noise-ratio is  $SNR = 100$ . All velocities given in this article are heliocentrically corrected using the correction given by the MIDAS routine COMPUTE/BARY ( $\delta v_{\oplus}$  in Table 2).

**Table 1.** Observational parameters of HD 56126 (SAO 96709, IRAS 07134+1005)

		Remark
Sp.T	F5I	Nassau <i>et al.</i> 1965
Sp.T	G5	HD catalogue (1919)
$T_{\text{eff}}$	6500 K	Parthasarathy <i>et al.</i> 1992
$\log g$	-1.4	Parthasarathy <i>et al.</i> 1992
$\alpha$	07 <sup>h</sup> 13 <sup>m</sup> 25.30 <sup>s</sup>	B1950
$\delta$	+10°05'09"	B1950
$l^{\text{II}}$	206.75°	
$b^{\text{II}}$	+9.99°	
$V$	8.23	Hrivnak <i>et al.</i> 1989
$B$	9.13	Hrivnak <i>et al.</i> 1989
$(B - V)_{\circ}$	0.30	F5I
$E(B - V)$	0.60	
$v_{\star\text{CO}}$	$85.6 \pm 1.0 \text{ km s}^{-1}$	CO millimeter emission
$\delta v_{\odot}$	$-14.11 \text{ km s}^{-1}$	helio $\rightarrow$ lsr

The conversion between different coordinate systems is made according to Eq. 1 and 2, where  $v_{\oplus}$  is the observed velocity and  $\delta v_{\oplus}$  the correction term to the heliocentric coordinate system ( $v_{\odot}$ ). Adding an extra term of  $\delta v_{\odot}$ , gives the velocity in the Local Standard of Rest system ( $v_{\text{lsr}}$ ).

$$v_{\odot} = v_{\oplus} + \delta v_{\oplus} \quad (1)$$

$$v_{\text{lsr}} = v_{\odot} + \delta v_{\odot} \quad (2)$$

### 3. Spectral line identification

#### 3.1. Introduction

In this section we will investigate which types of spectral lines are found in the optical spectrum of HD 56126. The spectral lines are classified in different categories: those from molecular species (e.g. C<sub>2</sub> and CN) and those from atoms. The atomic absorption lines are subdivided in those from the stellar photosphere (e.g., Cl, Ni, and OI) and those formed by circum- or interstellar gas (e.g., NaI D).

#### 3.2. Molecular absorption lines

The first detection of interstellar C<sub>2</sub> was made by Souza and Lutz (1977) and the first detection of interstellar CN by Dunham (1941). Since then C<sub>2</sub> and CN and many other molecules have been observed in dense interstellar clouds in the line of sight of a dozen bright stars (Van Dishoeck and De Zeeuw 1984). Photospheric molecular line absorption has been observed by Bergeat *et al.* (1976) and Barnbaum (1994) among others in the optical spectra of cool carbon stars. A list of molecular bands of a number of astrophysically interesting molecules can be found in Wallace (1962).

We have identified the vibrational (1,0), (2,0), and (3,0) bands of the C<sub>2</sub> Phillips system (A<sup>1</sup>Π<sub>u</sub> – X<sup>1</sup>Σ<sub>g</sub><sup>+</sup>), the (0,0) and (1,0) C<sub>2</sub> Swan bands (d<sup>3</sup>Π<sub>g</sub> – a<sup>3</sup>Π<sub>u</sub>), and the vibrational (1,0), (2,0), (3,0), and (4,0) bands of the “Red system” of CN (A<sup>2</sup>Π – X<sup>2</sup>Σ<sup>+</sup>) in the optical spectrum of HD 56126. Although we expect C<sub>3</sub> (Hrivnak 1995) in the optical spectrum, we were not able to detect this, since the C<sub>3</sub> A<sup>1</sup>Π<sub>u</sub> – X<sup>1</sup>Σ<sub>g</sub><sup>+</sup> at 4050 Å is not in the wavelength range observed. The presence of CH<sup>+</sup> could not be proven for the same reason. Table 3 gives an overview of the molecular bands identified, while line identification lists of several vibrational bands are given in App. A (only available at CDS).

The formation of C<sub>2</sub> and CN are both thought to be due to photo-dissociation of more complex molecules by the ultraviolet radiation field (e.g., Cherchneff *et al.* 1993). In the case of C<sub>2</sub> the photo-dissociation reaction is given by C<sub>2</sub>H<sub>2</sub> → C<sub>2</sub>H → C<sub>2</sub>, while in the case of CN we have the photo-dissociation reaction HCN → CN. We note that the HCN abundance in this object is quite small (Omont *et al.* 1993). We have calculated the ratio between the IS UV flux (Draine 1978) and the stellar UV flux (T<sub>eff</sub> = 6500 K Kurucz model). At a typical distance of the AGB remnant,  $r \geq 10^{16}$  cm, the stellar UV radiation field is about a factor 10<sup>4</sup> more intense (in the number of available UV photons) than the interstellar UV radiation

flux for  $\lambda \leq 2000$  Å. Therefore the layers where C<sub>2</sub> and CN exist are probably on both the inner and outer radius confined by photo-dissociation processes. When the star evolves along the post-AGB to higher temperatures, the stellar UV field increases in intensity and the inner radius of the C<sub>2</sub> and CN layers will move outwards. Due to the absence of a proper chemical model for the circumstellar chemistry of post-AGB stars, we will use the model for the AGB star IRC+10216 (Cherchneff *et al.* 1993).

Molecules can exist at low temperatures like in the photosphere of carbon stars and in interstellar clouds (T<sub>gas</sub> ≤ 3000 K). It is obvious that these conditions do not hold in the photosphere of HD 56126 with an effective temperature of T<sub>eff</sub> = 6500 K. Our conclusion is thus that the molecular lines are not photospheric but inter- or rather circumstellar. This idea is sustained by the fact that the heliocentric radial velocity of the molecular absorption lines is  $-8.5 \pm 0.6$  km s<sup>-1</sup> blue-shifted with respect to the central velocity (system velocity of HD 56126) derived from the molecular line emission (CO lines: see Table 11).

The average velocities for different bands of different molecules are the same (Table 10). The only exception is the Phillips (1,0) band which has an average velocity 6 km s<sup>-1</sup> higher than the other bands. We determined velocities of photospheric lines in the same wavelength region and found a similar shift of 6 to 10 km s<sup>-1</sup> with respect to photospheric lines at shorter wavelengths. Since no accurate wavelength information of the ThAr lamp was available for wavelengths longer than 9648 Å at the time of reducing the spectra, the wavelength calibration of this part of the spectrum was obtained by extrapolation of the wavelength calibration fit. For wavelengths longer than 6548 Å the wavelength calibration is less accurate, and the difference in velocity of the Phillips (1,0) is due to an error in the wavelength calibration.

In this article we have identified those molecular bands which are clearly present in the spectrum. But there are also bands present which can only be found by studying a small part of the spectrum in detail. In the process of identifying the CN (3,0) band another molecular band was found. So far it has not been possible to make an identification, but the lines are also present in a spectrum obtained in December 1993, and they are shifted in wavelength. This excludes a telluric origin and favors the idea that these lines are from circumstellar origin. Table 4 gives the observed wavelength and equivalent width of the unidentified molecular lines with a depression larger than 5%. The third column gives the predicted laboratory wavelength in air assuming that the line-forming region is the same as for C<sub>2</sub> and CN.

#### 3.3. Atomic line absorption

An abundance study by Klochkova (1995) using optical echelle spectra while assuming LTE and hydrostatic equilibrium showed that HD 56126 has an overabundance of

**Table 2.** Log of the UES observations ( $R \approx 5.2 \times 10^4$ ) of HD 56126

Day	Date		Int. time [sec.]	Air mass	Wavelength [Å]	$\delta v_{\oplus}$ [km s <sup>-1</sup> ]
	U.T.					
24/02/1992	21:39		600	1.06	4430 - 6887	-21.20
24/02/1992	21:57		600	1.06	5409 - 10302	-21.34

**Table 3.** Identified molecular bands in the optical spectrum of HD 56126

Molecule	System	Band	Wavelength range [Å]		Remark
C <sub>2</sub>	Phillips	A <sup>1</sup> Π <sub>u</sub> – X <sup>1</sup> Σ <sub>g</sub> <sup>+</sup>	(1,0)	10137	10213
C <sub>2</sub>	Phillips	A <sup>1</sup> Π <sub>u</sub> – X <sup>1</sup> Σ <sub>g</sub> <sup>+</sup>	(2,0)	8753	8913
C <sub>2</sub>	Phillips	A <sup>1</sup> Π <sub>u</sub> – X <sup>1</sup> Σ <sub>g</sub> <sup>+</sup>	(3,0)	7717	7809
C <sub>2</sub>	Swan	d <sup>3</sup> Π <sub>g</sub> – a <sup>3</sup> Π <sub>u</sub>	(0,0)	5100	5166
C <sub>2</sub>	Swan	d <sup>3</sup> Π <sub>g</sub> – a <sup>3</sup> Π <sub>u</sub>	(1,0)	4710	4740
CN	Red system	A <sup>2</sup> Π – X <sup>2</sup> Σ <sup>+</sup>	(1,0)	9142	9202
CN	Red system	A <sup>2</sup> Π – X <sup>2</sup> Σ <sup>+</sup>	(2,0)	7874	7918
CN	Red system	A <sup>2</sup> Π – X <sup>2</sup> Σ <sup>+</sup>	(3,0)	6927	6954
CN	Red system	A <sup>2</sup> Π – X <sup>2</sup> Σ <sup>+</sup>	(4,0)	6190	6225

**Table 4.** List of unidentified molecular lines

$\lambda_{\text{obs}}$ [Å]	$W$ [mÅ]	$\lambda_{\text{lab}}^{\text{predicted}}$ [Å]	remark
6911.7	33.1	6909.4	
6912.6	49.8	6910.3	blend (band head?)
6912.8	24.9	6910.5	blend
6914.6	15.1	6912.3	
6915.0	23.1	6912.7	
6917.3	25.5	6915.0	
6920.2	10.9	6917.8	
6921.9	29.7	6919.6	
6924.9	30.2	6922.6	
6925.8	18.2	6923.5	
6930.8	22.0	6928.5	

CNO and the heavy elements, and a large excess of all s-process elements. This abundance pattern is expected for a post-AGB star which has experienced the third dredge-up on the AGB.

We have analyzed the optical photospheric spectrum and found that almost all lines are asymmetric. A recent study by Oudmaijer and Bakker (1994) shows that most photospheric lines, e.g., H $\alpha$ , FeI and FeII, etc., show changes in absorption line profiles on time scales of less than a month. They attribute this to a pulsation of the photosphere with a period shorter than 65 days. If the pulsation scenario is correct, this will raise questions about the interpretation of the abundance studies: pulsation

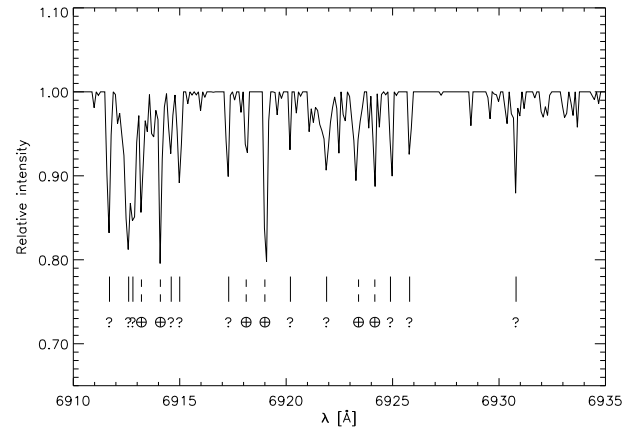


**Fig. 3.** An unidentified molecular band. The “?” signs denote unidentified lines, whereas an “⊕” denotes a telluric line which was not completely removed by dividing the spectrum by the reference stars HR 4049. All lines with a depression of  $\geq 5\%$  are significant.

could give an emission component in the absorption features and thus change the observed equivalent width in a complicated way.

### 3.3.1. CI, NI, and OI absorption lines

To allow an accurate determination of the photospheric velocity we have fitted Gaussians to the line profile of se-

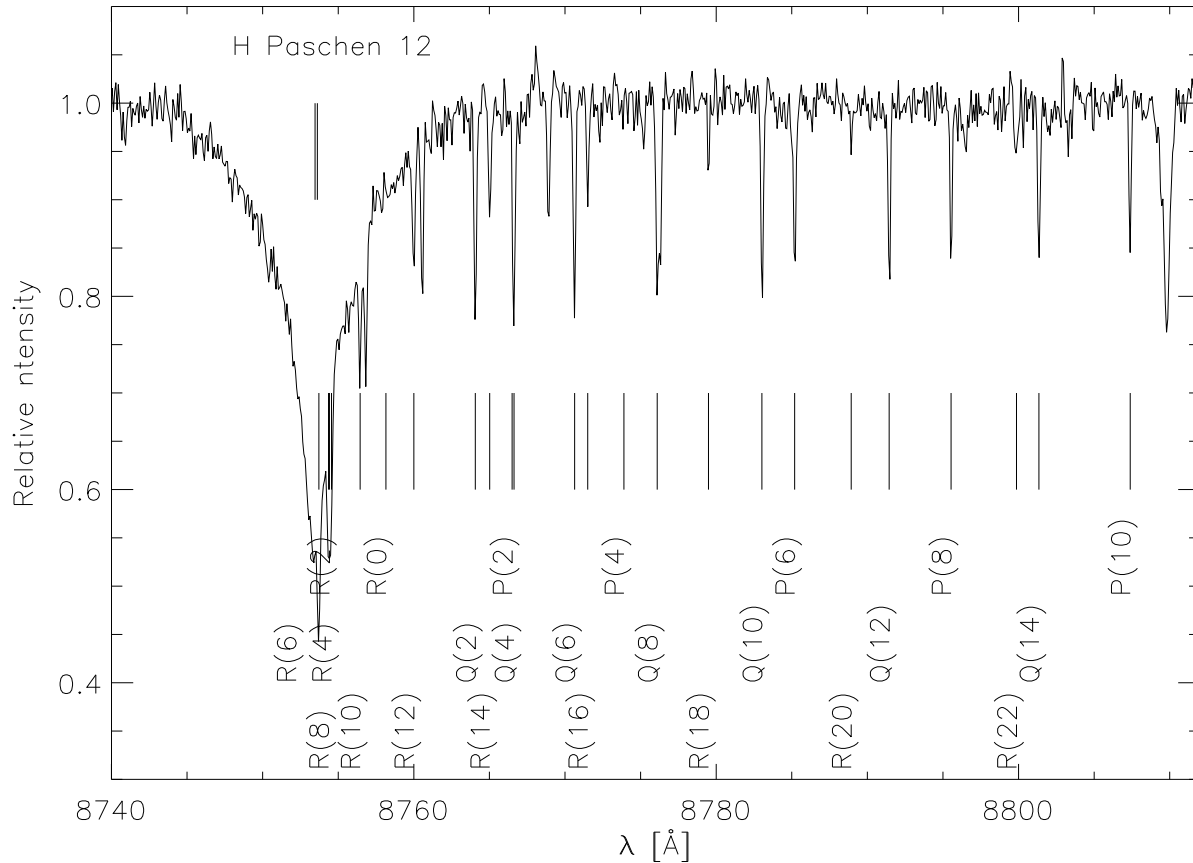


**Fig. 1.** The Phillips (2,0) band in the spectrum of HD 56126. The C<sub>2</sub> transitions are recognized by the narrow absorption profiles (not resolved). The photospheric absorption line at 8809.8 Å is the MgI(7) transition.

lected CI, NI and OI lines. As the lines are asymmetric in shape we have fitted the profiles using the core of the feature as the most important fitting criteria. A list of identification, equivalent width and depth of the lines is presented in App. B (at CDS) and the results are summarized in Table 5.

The photospheric radial velocity thus obtained,  $82.3 \pm 0.6 \text{ km s}^{-1}$ , is almost equal to the average central velocity of the CO line emission of  $85.6 \pm 0.5 \text{ km s}^{-1}$  (Nyman *et al.* 1992 and Bujarrabal *et al.* 1992). The small difference of  $3.3 \text{ km s}^{-1}$  is probably caused by pulsation of photosphere: the star is in a phase of expansion.

### 3.3.2. The absorption components in the NaI D lines

In view of the fact that the AGB remnant is cool (dust temperatures of about  $T_{\text{dust}} = 200 \text{ K}$ ), the spectral features most likely to have a contribution from circumstellar material are the resonance absorption lines. For this study we have chosen the NaI D doublet. HD 56126 has a strong

**Table 5.** Velocities of photospheric absorption lines

Ion (multiplet)	$\chi$ [eV]	Number of lines	$v_{\odot}$ [ $\text{km s}^{-1}$ ]
CI	$\geq 7.45$	3	$80.7 \pm 0.8$
NI	$\geq 10.28$	1	83
OI	$\geq 9.11$	3	$83.7 \pm 0.3$
average	$\geq 7.45$	7	$82.3 \pm 0.6$

infrared excess and will probably show both an inter- and circumstellar contribution in the NaI D lines.

A similar study has been made of the NaI D lines profiles in the spectra of Planetary Nebulae (Dinerstein *et al.* 1995). They have shown that there is a circumstellar component present in the lines profiles of the NaI D lines.

The NaI D1 (5895.923 Å) and D2 (5889.953 Å) lines in the spectrum of HD 56126 show a very complex structure

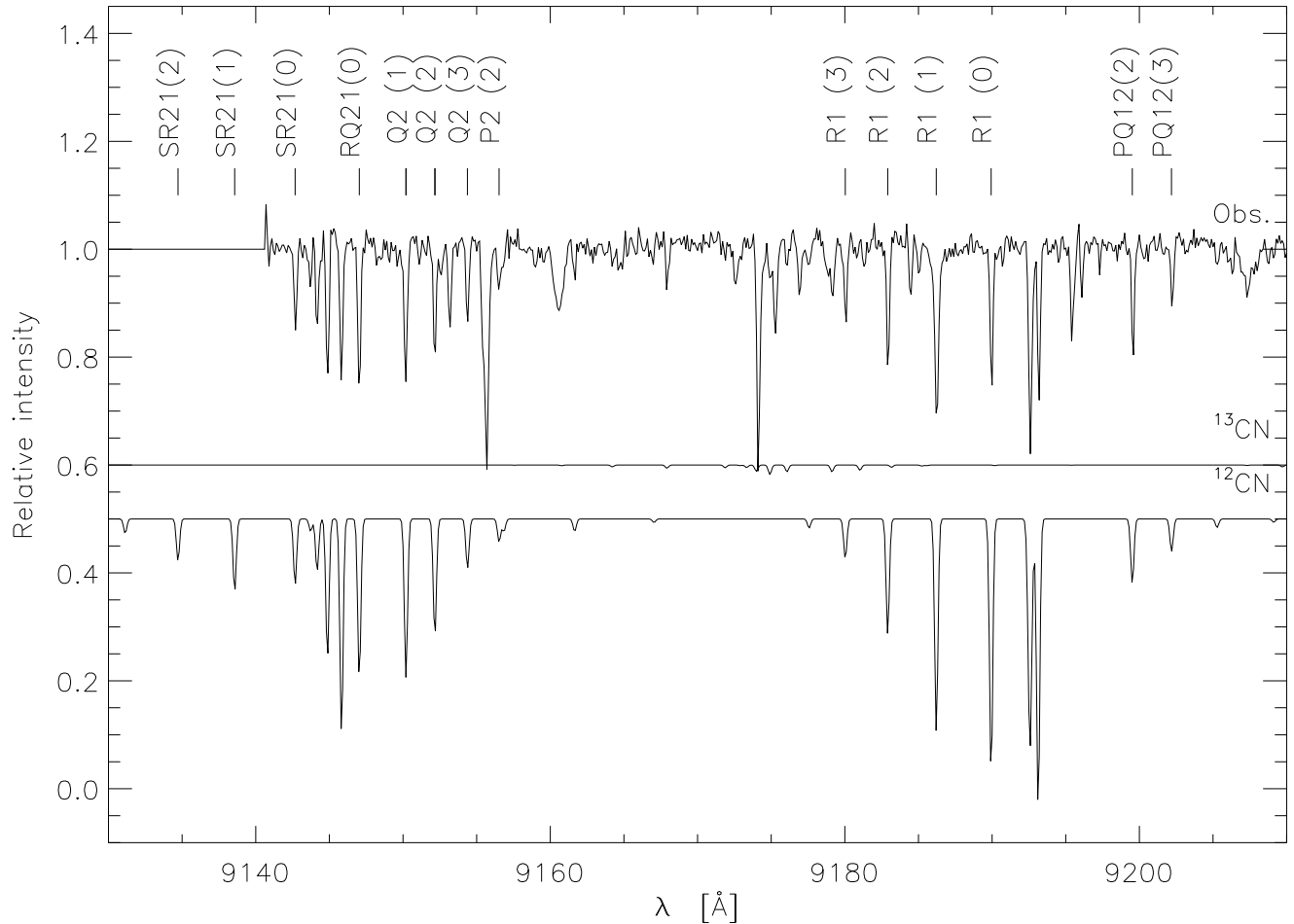


**Fig. 2.** The observed spectrum at the CN  $A^2\Pi - X^2\Sigma^+$  (1,0) band. The spectrum has been divided by a template spectrum to remove the telluric lines. A synthetic spectrum ( $T_{\text{rot}} = 13$  K and  $N_{\text{Boltz}} = 13.9 \times 10^{14} \text{ cm}^{-2}$ ) has been calculated to help to identify the absorption lines. The  $^{13}\text{C}^{14}\text{N}$  spectrum is shifted down by 0.4 and the  $^{12}\text{C}^{14}\text{N}$  spectrum by 0.5 ( $^{12}\text{C}/^{13}\text{C} = 25$ ). The strongest (not blended) molecular lines are marked with their identification (with  $N''$  number). The features at 9155 and 9174 Å are artifacts from the template spectrum.

(Fig. 4). By comparing the profile of the D1 line with the D2 line we can see which absorption features are real and which are artifacts. At least six different components could be identified. The four most blue-shifted components form one broad feature, while the two other components form a second less blue-shifted broad feature. In fitting Gaussian profiles to all components with the exception of the photospheric component (no. 6) we have determined the velocities of the individual components in the D1 and D2 lines independently. After extracting five Gaussian profiles, we have assumed that the residual of the spectrum is the photospheric contribution. The velocity of the latter contributor is determined with an eyeball fit. A summary of the determined velocities from the NaI D1 and D2, and C<sub>2</sub> and CN lines are given in Table 6. The error on the individual velocities is about  $3 \text{ km s}^{-1}$ . The only exception is the velocity of component 6, as this is the only component which was isolated after subtracting of the other.

The estimated error on the velocity of component 6 is  $6 \text{ km s}^{-1}$ .

### 3.4. Conclusions

At this stage we note that the Doppler velocity found for the C<sub>2</sub> and CN molecules is equal to the velocity found for the NaI Comp 5. This suggests that they are formed in the same region. Comp 6 is very close to the photospheric velocity. In Sect. 5 we will use the Galactic rotation curve to distinguish between the interstellar, circumstellar, and photospheric contribution and argue that the NaI D1 and D2 components 1, 2, 3, and 4 are probably interstellar. C<sub>2</sub>, CN, and the NaI D component no. 5 are thought to be of circumstellar origin. The NaI D component 6 is of photospheric origin.

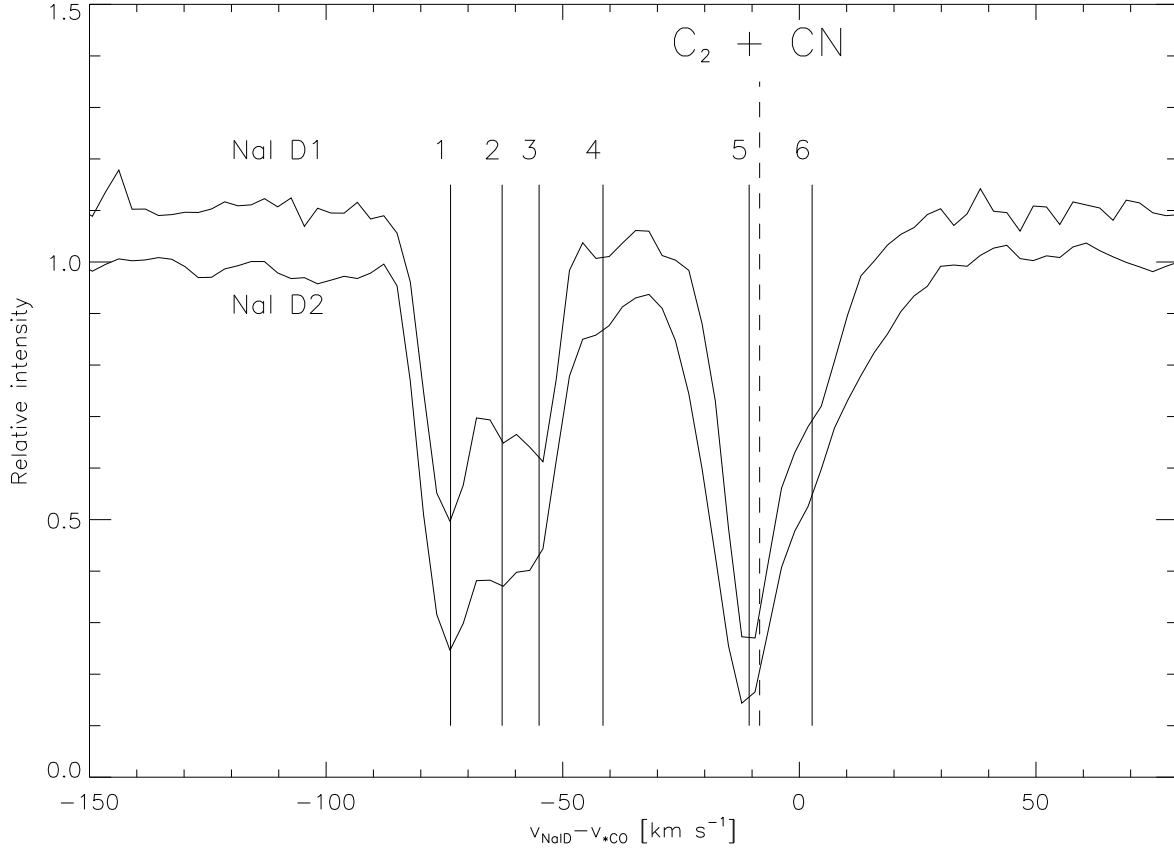


**Fig. 4.** The NaI D1 (top, shifted by 0.1 in relative intensity) and D2 (bottom) absorption profiles show two well-separated broad components. The most blue-shifted profile is of interstellar origin and shows at least four different components (no. 1 to 4). The less blue-shifted profile has the large contribution from the AGB wind (no. 5). Component no. 6 is photospheric.

**Table 6.** Doppler (heliocentric) velocities and equivalent width of the six components in the absorption profile of the NaI D1 and D2 lines. The data on molecular lines absorption is given for comparison. The average CO velocity of  $85.6 \pm 0.5$  km s<sup>-1</sup> has been used to determine the outflow velocity.

no.	$v_{D1}$ [km s <sup>-1</sup> ]	$W_{D1}$ [mÅ]	$v_{D2}$ [km s <sup>-1</sup> ]	$W_{D2}$ [mÅ]	$v_{NaI D}$ [km s <sup>-1</sup> ]	$v_D - v_{*CO}$ [km s <sup>-1</sup> ]	remark	
1	$12 \pm 3$	$154 \pm 5$	$12 \pm 3$	$218 \pm 16$	$12 \pm 2$	$-73.8 \pm 2.0$	IS	
2	$23 \pm 3$	$55 \pm 5$	$23 \pm 3$	$67 \pm 18$	$23 \pm 2$	$-62.9 \pm 2.0$	IS	
3	$30 \pm 3$	$90 \pm 5$	$31 \pm 3$	$114 \pm 6$	$31 \pm 2$	$-55.1 \pm 2.0$	IS	
4	$44 \pm 3$	$16 \pm 5$	$44 \pm 3$	$33 \pm 5$	$44 \pm 2$	$-41.6 \pm 2.0$	IS	
5	$75 \pm 3$	$240 \pm 5$	$75 \pm 3$	$316 \pm 23$	$75 \pm 2$	$-10.7 \pm 2.0$	CS	
6	$89 \pm 6$	$103 \pm 10$	$87 \pm 6$	$87 \pm 10$	$88 \pm 4$	$+2.6 \pm 2.0$	Ph	
					$v$ [km s <sup>-1</sup> ]	$v_* - v_{*CO}$ [km s <sup>-1</sup> ]		
					CO	$85.6 \pm 0.5$	0.0	CS
					C <sub>2</sub> and CN	$77.1 \pm 0.3$	$-8.5 \pm 0.6$	CS

$v$ : heliocentrically corrected radial velocity;  $W$ : the equivalent width

## 4. Physical conditions of line-forming region of molecular line absorption

### 4.1. Introduction

An analysis of the spectra of molecular bands allows the deduction of chemical composition, rotational temperatures, column densities, and radial velocities of the line-forming region. Examples of the detection of molecular bands are shown in Figs. 1 and 2. From these figures we see immediately that these molecular lines are not resolved by the instrument. The width of the molecular absorption lines is much smaller than the width of the observed photospheric (e.g., CI, NI, OI) lines.

In this section we look in detail at the physical conditions occurring in the molecular line-forming region by an analysis of the molecular bands. Only in the case of an optically thin medium can the rotational temperature and the column density (assuming a Boltzmann distribution over the  $J''$  levels) be derived in a simple way. In the optically thin case there is a linear relation between the observed equivalent width and population density of the lower level of the transition. Using simple formulae this gives the rotational temperature and the column density. In this discussion we will focus on the C<sub>2</sub> Phillips bands, but the same technique can be applied to CN. Data of the CN bands was extracted from the SCAN-CN tape of Jørgenson and Larson (1990).

In order to describe the method of deriving physical parameters from the observations, we discuss the notation for the rotational levels and lines of diatomic molecules (Whiting 1973). A transition is denoted by  $(v'J', v''J'')$  where the first index,  $v'J'$ , is the upper level and the second index,  $v''J''$ , the lower level.  $v$  and  $J$  denote the vibrational and rotational quantum number respectively. Since we only consider the Phillips bands, all transitions are between the same electronic states, from  $X^1\Sigma_g^+$  to  $A^1\Pi_u$ , and we observe different vibrational bands  $(v', v'')$ : (1,0), (2,0), and (3,0). Each vibrational band consists of numerous lines from rotational transitions  $(J', J'')$ . The difference in oscillator strength between the vibrational bands is expressed in the band oscillator strength. In deriving physical parameters from the observations we will make use of optically thin lines. The (3,0) vibrational band of C<sub>2</sub> is weaker than the (1,0) and (2,0) vibrational band. This makes the (3,0) more suitable for our analysis than the (2,0) and (1,0) vibrational band.

### 4.2. Rotational diagram

#### 4.2.1. Case of C<sub>2</sub>

In the optically thin case ( $\tau \ll 1$ , where the absorption lines are on the linear part of the curve of growth) the

column density for molecules in the  $(J', J'')$  transition is given by Eq. 3.

$$N_{v''J''} [\text{cm}^{-2}] = 1.13 \times 10^{17} \frac{W_\lambda^{J'J''} [\text{m}\text{\AA}]}{f_{J'J''} \lambda_{J'J''}^2 [\text{\AA}]}, \quad (3)$$

with  $W_\lambda^{J'J''}$  the observed equivalent width in mÅ,  $f_{J'J''}$  the oscillator strength as given by Eq. 7, and  $\lambda_{J'J''}$  the vacuum wavelength of the  $(J', J'')$  transition.

The oscillator strength  $f_{J'J''}$  is calculated (Eq. 7) from the tabulated band oscillator strength  $f_{v'v''}$  (Table 8), the band head  $\nu_{\text{band}}$  (Table 8), the computed values for the frequency of the transition,  $\nu_{J'J''}$ , and the normalized Hönl-London factors (line intensity factor),  $S_{J'J''}$ . The Hönl-London factors for the C<sub>2</sub> Phillips bands were computed for the A-X system ( $\Delta\Lambda = 1$ ). The general formulae for the Hönl-London factors (Herzberg 1950) are simplified to Eq. 4, 5, and 6 and normalized such that for each  $J''$ ,  $\sum_{J'} \frac{S_{J'J''}}{g_e''/g_e'(2J''+1)} \equiv 1$ .

$$S_{J''}^P = (J'' - 1) \quad (4)$$

$$S_{J''}^Q = (2J'' + 2) \quad (5)$$

$$S_{J''}^R = (J'' + 2) \quad (6)$$

$$f_{J'J''} = f_{v'v''} \left[ \frac{\nu_{J'J''}}{\nu_{\text{band}}} \left( \frac{S_{J'J''}}{g_e''/g_e'(2J''+1)} \right) \right], \quad (7)$$

with  $g_e''/g_e'$  the ratio of electronic degeneracy factor. For the C<sub>2</sub> and CN A-X system  $g_e''/g_e' = 2$ . Each rotational level has degeneracy of  $(2J''+1)$ , and the energy of the lower rotational level is given by  $E_{J''}$  (Eq. 9). It should be noted that as C<sub>2</sub> is a homo-nuclear molecule without a permanent dipole moment, symmetry of rotational states does not allow odd-numbered rotational levels in the  $X^1\Sigma_g^+$  electronic state to exist. The absorption oscillator strength and laboratory wavelength in air for the lines used in the analyses are given in App. A (at CDS).

If we apply Eq. 3 to lines which are not optically thin, we underestimate the column density. This is clearly demonstrated in the computed column densities for low  $J''$  values of the Phillips (1,0) band (see App. A). In the case of optically thin lines the column density derived for a given  $J''$  value should be the same for the P, Q, and R branch lines. But in the case of optically thick lines the column density derived from the Q branch line is the lowest while the column density from the P branch line is the highest (lowest  $f_{J'J''}$ ).

By assuming a Boltzmann distribution over the rotational levels the population density of level  $J''$  is given by

$$N_{v''J''} = \frac{N_{\text{Boltz}}}{Q_r} (2J'' + 1) \exp\left(\frac{-E_{J''}}{kT_{\text{rot}}}\right) \quad (8)$$

with

$$\frac{E_{J''}}{k} = \frac{B_e h c}{k} J'' (J'' + 1) [\text{K}] \quad (9)$$



**Table 7.** Molecular parameters

Parameter	C <sub>2</sub>	CN
	A <sup>1</sup> Π <sub>u</sub> – X <sup>1</sup> Σ <sub>g</sub> <sup>+</sup>	A <sup>2</sup> Π – X <sup>2</sup> Σ <sup>+</sup>
B <sub>e</sub> [cm <sup>-1</sup> ]	1.820101	1.8996
Herzberg 1950		

**Table 8.** Molecular parameters used in this work to calculate the oscillator strength  $f_{J',J''}$ . Items which are not used in this work are intentionally left blank.

band	$\nu_{\text{band}}(\text{vac})$ [cm <sup>-1</sup> ]	$f_{v',v''}$	ref. λ
Phillips (1,0)	9854.0247 <sup>(1)</sup>	2.84 10 <sup>-3</sup> <sup>(2)</sup>	1
Phillips (2,0)	11413.8250 <sup>(1)</sup>	1.67 10 <sup>-3</sup> <sup>(2)</sup>	1
Phillips (3,0)	12947.81 <sup>(3)</sup>	7.52 10 <sup>-4</sup> <sup>(2)</sup>	1
Swan (0,0)		1.5 10 <sup>-3</sup> <sup>(5)</sup>	4
Swan (1,0)		7.6 10 <sup>-3</sup> <sup>(5)</sup>	4
CN (1,0)		1.50 <sup>(5)</sup>	6
CN (2,0)		0.76 <sup>(5)</sup>	6
CN (3,0)		0.28 <sup>(5)</sup>	6
CN (4,0)			6

1: Chauville *et al.* 1977; 2: Van Dishoeck 1983; 3: Ballik and Ramsay 1976; 4: Amiot 1983; 5: Davis *et al.* 1986; 6: Jørgenson and Larson 1990

and

$$Q_r = \sum_{J''}^{\infty} (2J'' + 1) \exp \frac{-E_{J''}}{kT_{\text{rot}}} . \quad (10)$$

$B_e$  represents the rotational constant of the lower electronic level (Table 7), and  $k$ ,  $h$ , and  $c$  the Boltzmann, Planck constant, and the velocity of light respectively.

The rotational diagram with on the vertical axis  $\ln(N_{J''}/(2J'' + 1))$  and on the horizontal axis  $E_{J''}/k$  has a slope of  $a = -1/T_{\text{rot}}$  and an offset of  $b = \ln(N_{\text{Boltz}}/Q_r)$ . Thus the temperature is given by the slope, and the column density is given by the offset of the first order fit in the rotational diagram.

The effect of optical depth on the derived column densities can be seen in the rotational diagrams (Fig. 5). In the rotational diagram of the (1,0) band, the Q branch lines lie lower than the P branch lines. In the case of the (2,0) band one should note that the R branch lines (squares) up to  $J'' = 12$  are blended with the Paschen 12 line. If we do not take into account R( $J'' = 0, 2, 4, 6, 8, 10, 12$ ), then we notice that also for the (2,0) band the Q branch lines lie lower than the P branch lines. In the rotational diagram of the (3,0) band we do not see a systematic difference in column density between the different branches. Based on the derived column densities for

the P, Q, and R branch lines, we conclude that the (1,0) and (2,0) band are optically thick while the (3,0) band is optically thin.

The population density of the  $J''$  rotational levels does not decrease monotonically with  $J''$ , it reaches a maximum where the population decreases due to an increase of rotational energy of the levels ( $E_{J''}$ ), and the population increases due to an increase of degeneracy of the level ( $2J'' + 1$ ). This means that the highest optical depth for  $T_{\text{rot}} \approx 242$  K is reached around  $J'' = 8, 10, 12$ , and a local minimum is observed in the rotational diagram. At low  $J''$  values (e.g.  $J'' = 0, 2$ ) and at high  $J''$  values ( $J'' \geq 18$ ) the (1,0) and (2,0) vibrational bands are optically thin.

From the derived column densities of the rotation levels  $J''$  of the (3,0) band, we can compute the rotational temperature and the column density of the vibration level  $v''$ . In doing this we assume that the population distribution over the rotational levels follows a Boltzmann distribution. Since the rotational diagram of the optically thin vibrational band (3,0) gives a straight line, the approximation is to first order allowed. It should be noted that this does not necessarily mean that  $T_{\text{kin}} = T_{\text{rot}}$  as the excitation of the molecule is due to the combined effect of collisional and radiative (de-)excitation. In the case of a homo-nuclear specie like C<sub>2</sub>  $T_{\text{rot}} \geq T_{\text{kin}}$ , while for a hetero-nuclear specie like CN  $T_{\text{rot}} \leq T_{\text{kin}}$ . Detailed modeling is required to find  $T_{\text{kin}}$  from the molecular excitation.

#### 4.2.2. Case of CN

In the case of CN the spin angular momentum  $S$  is decoupled from the total angular momentum and the energy levels are described by the total angular momentum quantum number  $N$ . Eq. 3 is valid for CN when  $J''$  is replaced by  $N''J''$ . Then  $N_{v'',N''}$  is given by  $N_{v'',N''J''}$  summed over the  $J'' = N'' - 1/2$  and  $J'' = N'' + 1/2$  levels (Table 9). Eqs. 8, 9, and 10 are also valid when  $J''$  is replaced by  $N''$ .

**Table 9.** The observed column densities (in units of 10<sup>12</sup> cm<sup>-2</sup>) of the CN Red system

$N''$	$J''$	(1,0)	(2,0)	(3,0)
0	1/2	130	200	420
1	1/2	116	240	328
1	3/2	174	?	412
2	3/2	176	225	256
2	5/2	160	221	377
3	5/2	81	158	388
3	7/2	110	?	?

The calculation of the oscillator strength for CN using an equation analogue to Eqs. 4, 5, 6, and 7 is not trivial,

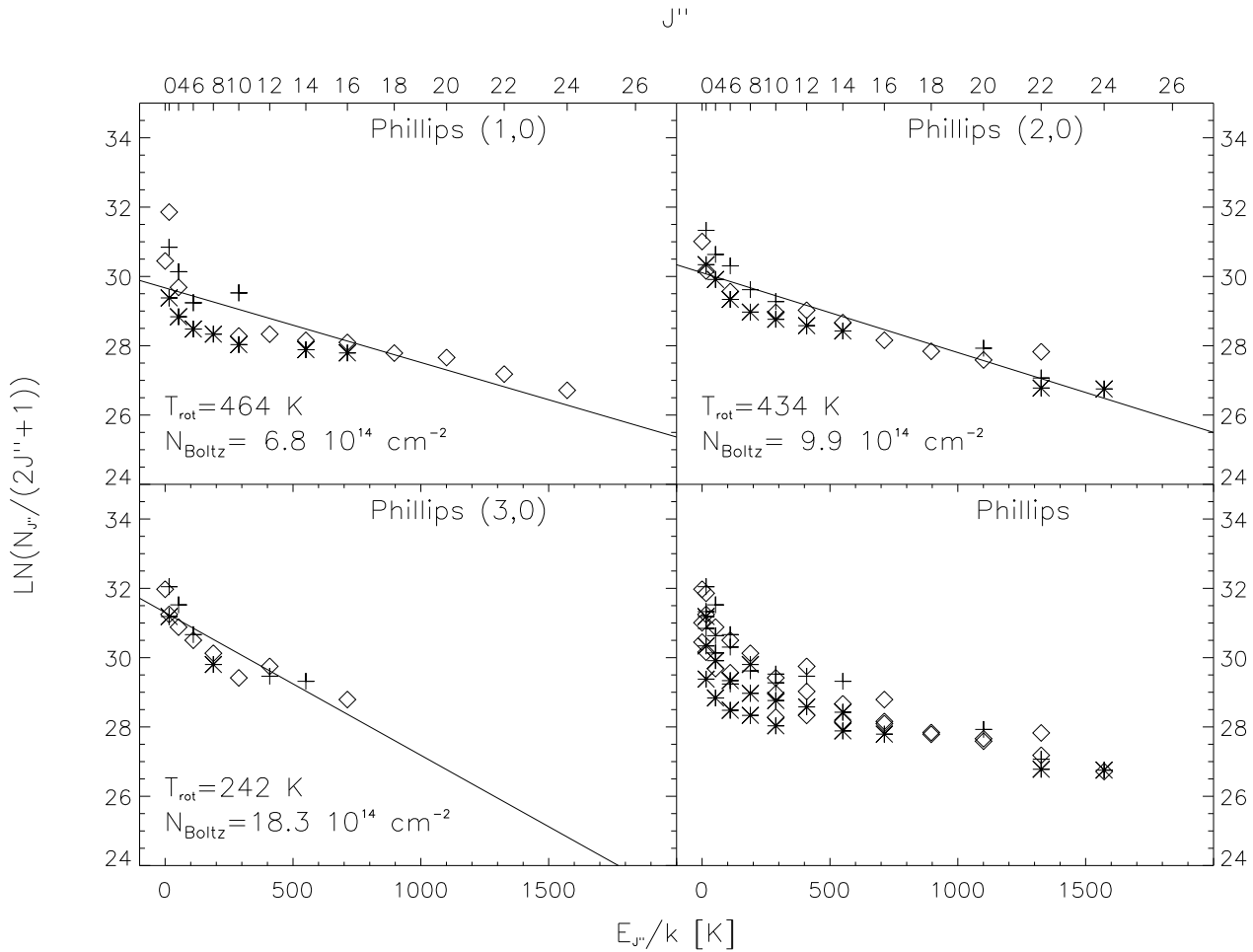


**Fig. 5.** Rotational diagram of the Phillips (1,0), (2,0), and (3,0) bands. The P, Q, and R branch lines are denoted by a plus, asterisk, and square respectively. Only the weakest rotational band (3,0) is optically thin and gives an almost linear relation in the rotational diagram.

and we have therefore adopted the  $\log gf$  values for CN of the SCAN-CN tape. The  $\log gf$  values have been multiplied by a factor of 0.734 as suggested by the authors of the tape. For a detailed description of CN and further reading we refer to Jørgenson and Larson (1990).

#### 4.3. Determination of $T_{\text{rot}}$ , $N_{\text{Boltz}}$ and $N_{\text{observed}}$

Applying the Boltzmann law to derive a rotational temperature and column density of C<sub>2</sub> (Fig. 5) yields values ranging from  $T_{\text{rot}} = 242$  K to 464 K, and C<sub>2</sub> column densities of  $N_{\text{Boltz}} = 0.7$  to  $1.8 \times 10^{15}$  cm<sup>-2</sup>. These results are sensitive to the molecular lines and molecular bands included in the determination of the rotational temperature and the column density. The reason for this is that this method only gives valid results if the lines are optically thin and if the population density of the rotational levels can be described by a Boltzmann distribution.

As the (3,0) band is the only optically thin band and is most reliable for determining the rotational tempera-

ture and column densities, the values derived from this band will be adopted for the line-forming region:  $T_{\text{rot}} = 242 \pm 20$  K,  $N_{\text{Boltz}} = 1.8 \times 10^{15}$  cm<sup>-2</sup>. Using the same technique on the CN (3,0) band we find  $T_{\text{rot}} = 24 \pm 5$  K and  $N_{\text{Boltz}} = 3.3 \times 10^{15}$  cm<sup>-2</sup>. This gives a particle abundance ratio of  $f_{\text{C}_2}/f_{\text{CN}} = 0.5$  in reasonable agreement with the predicted molecular peak abundances ratio for the carbon-rich envelope of IRC +10216 of  $f_{\text{C}_2}/f_{\text{CN}} = 1.0$  (Cherchneff and Glassgold 1993). A second measure of the column density can be obtained by adding the observed column densities of each energy level. In that case we find for C<sub>2</sub> (3,0)  $N_{\text{obs}} = 2.0 \times 10^{15}$  cm<sup>-2</sup> and for CN (3,0)  $N_{\text{obs}} = 2.7 \times 10^{15}$  cm<sup>-2</sup>. This is reasonably in agreement in view of the fact that by adding the observed column densities only a limited number of levels are used, and that some of the observed lines will be optically thick.

A rotational temperature of 242 K for C<sub>2</sub> is significantly higher than expected for interstellar molecules ( $T_{\text{rot}} \leq 100$  K). The line-forming region is hotter than expected if it were in radiative equilibrium with the inter-

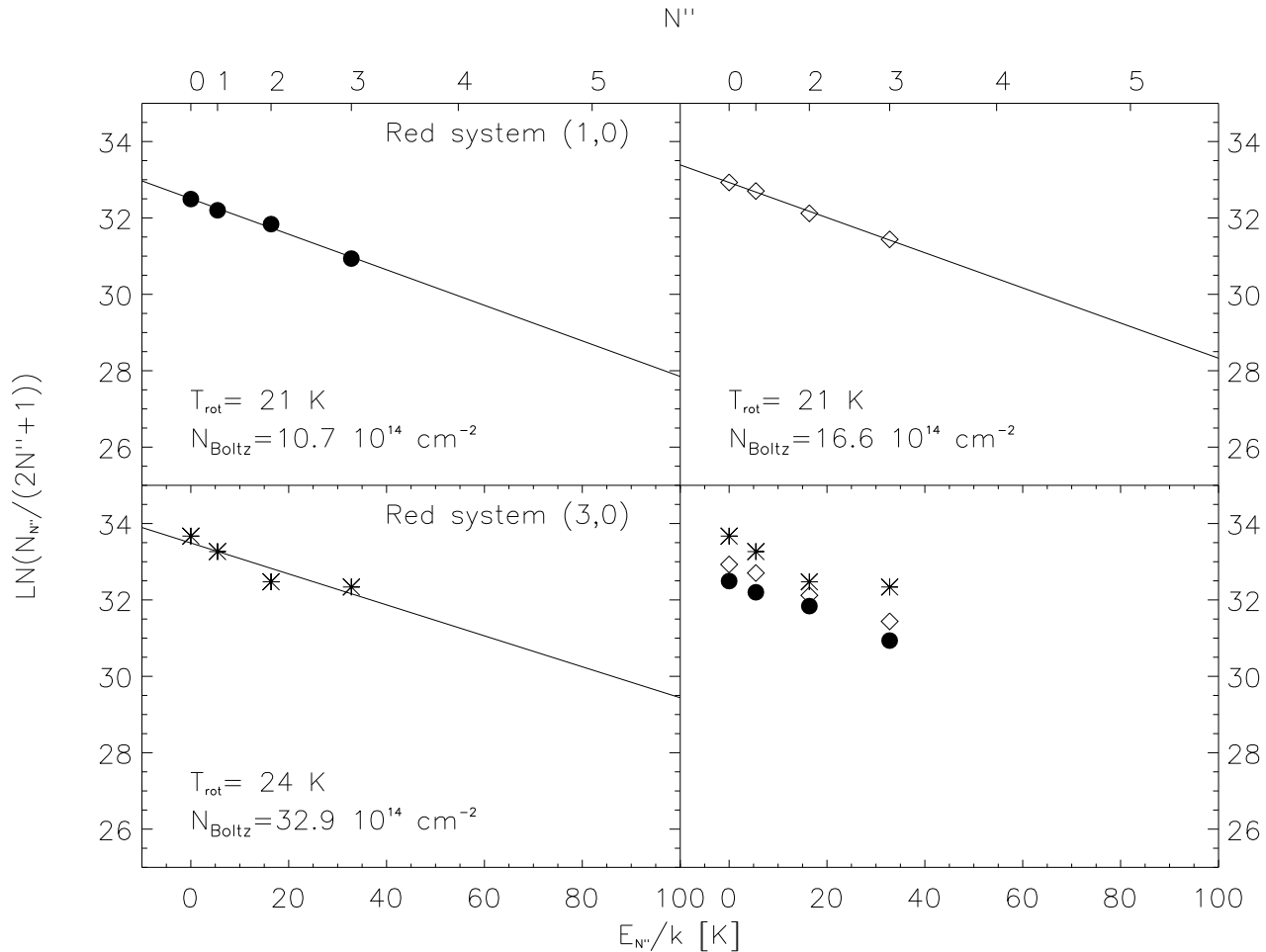


**Fig. 6.** Rotational diagram of the Red system of CN.

stellar radiation field, and this suggests that the molecules are in radiative equilibrium with the stellar radiation field. This is consistent with the velocity difference of  $-8.5 \pm 0.6 \text{ km s}^{-1}$  found between the millimeter line emission (CO) and the optical molecular line absorption and suggests that the line-forming region is circumstellar. This velocity difference is interpreted as the molecular outflow velocity. The fact that we only observe one velocity for the optically thin and optically thick lines of C<sub>2</sub> and CN suggests that the line-forming region is of constant velocity and that there is no significant velocity gradient.

### 5. Predicted velocities of interstellar absorption lines

In the former sections we have seen that the Doppler velocity of the molecular line absorption and the NaI D lines are not at the system velocity, but are from inter- or circumstellar origin. In this section we look at the predicted Doppler velocities for interstellar contributions. Using the simple argument that HD 56126 is located above the Galactic plane ( $b = 10^\circ$ ) with a relatively high helio-

centric radial velocity of  $85.6 \pm 0.5 \text{ km s}^{-1}$ , one expects to be able to distinguish interstellar from circumstellar contributions on the basis of observed velocities. We can estimate which observed Doppler velocities are probably not of interstellar origin.

From model evolutionary tracks (Schönberner 1983) one predicts for a typical post-AGB star with  $M_{\text{post-AGB}} = 0.6 M_\odot$ , a  $M_{\text{bol}} = -4.30$ . From the observations (Table 1) we find  $m_{\text{bol}} = 6.34$ , which places the star at a distance of 1.3 kpc and 0.2 kpc above the Galactic plane.

For the velocity structure of the Galactic disk we adopt the simple approximation given in Lang (1980) and subtract a correction term to convert to heliocentric velocities (Eq. 11). Inserting the Galactic coordinates of HD 56126 gives a formula which expresses the heliocentric radial velocity of the Galactic disk as a function of distance (Eq. 12).

$$v_\odot(\text{IS}) = -\delta v_\odot + A D \sin 2l \cos^2 b \text{ [ km s}^{-1} \text{]} \quad (11)$$

**Table 10.** Physical parameters derived from molecular bands

Band		$v_{\odot}$ [km s <sup>-1</sup> ]	$N_{\text{obs}}$ [10 <sup>14</sup> ]	$N_{\text{Boltz}}$ [cm <sup>-2</sup> ]	$T_{\text{rot}}$ [K]
C <sub>2</sub> Phillips	A <sup>1</sup> Π <sub>u</sub> – X <sup>1</sup> Σ <sub>g</sub> <sup>+</sup> (1,0)	82.7 ± 0.4	9.9	6.8	484
C <sub>2</sub> Phillips	A <sup>1</sup> Π <sub>u</sub> – X <sup>1</sup> Σ <sub>g</sub> <sup>+</sup> (2,0)	76.8 ± 0.2	12.3	9.9	434
C <sub>2</sub> Phillips	A <sup>1</sup> Π <sub>u</sub> – X <sup>1</sup> Σ <sub>g</sub> <sup>+</sup> (3,0)	76.7 ± 0.2	20.0	18.3	242
C <sub>2</sub> Swan	d <sup>3</sup> Π <sub>g</sub> – a <sup>3</sup> Π <sub>u</sub> (0,0)				
C <sub>2</sub> Swan	d <sup>3</sup> Π <sub>g</sub> – a <sup>3</sup> Π <sub>u</sub> (1,0)				
CN Red system	A <sup>2</sup> Π – X <sup>2</sup> Σ <sup>+</sup> (1,0)	77.7 ± 0.2	9.5	10.7	21
CN Red system	A <sup>2</sup> Π – X <sup>2</sup> Σ <sup>+</sup> (2,0)	76.3 ± 0.4	11.4	16.6	21
CN Red system	A <sup>2</sup> Π – X <sup>2</sup> Σ <sup>+</sup> (3,0)	78.0 ± 0.2	26.7	32.9	24
CN Red system	A <sup>2</sup> Π – X <sup>2</sup> Σ <sup>+</sup> (4,0)				
Average velocity		77.1 ± 0.3			

with the following parameters:

$$\delta v_{\odot} = -14.11 \text{ km s}^{-1}$$

$$A = 15 \text{ km s}^{-1} \text{ kpc}^{-1}$$

$$(l; b)_{\text{HD 56126}} = (206.75^{\circ}; 9.99^{\circ})$$

gives:

$$v_{\odot}(\text{IS}) = 14.11 + 11.69 \times D[\text{kpc}] \text{ [ km s}^{-1}\text{]} \quad (12)$$

Eq. 12 gives a lower- and upper-limit on the predicted velocities of interstellar lines using a distance of  $D = 0$  kpc and  $D = 1.3$  kpc respectively. We find a velocity range between 14 and 30 km s<sup>-1</sup>. That the lower limit is not zero is of course due to the motion of the sun with respect to the solar neighborhood. The upper limit of 30 km s<sup>-1</sup> is also the velocity expected for HD 56126 if it is of population I origin. The fact that there is a difference of 56 km s<sup>-1</sup> between “predicted” and observed velocity is the reason why HD 56126 is classified as a high-velocity star.

We can now look at Table 6 and distinguish the absorption components in the NaI D lines in two categories. We see that only components 2 and 3 are within the range expected for IS lines. As the predicted range of IS velocities is only a rough estimate, we argue that the whole absorption feature between heliocentric velocities of 10 and 44 km s<sup>-1</sup> (components 1,2,3, and 4) is probably of interstellar origin. This means that there are at least four independent interstellar clouds in the line of sight to HD 56126.

We can now immediately conclude that the absorption features with heliocentric velocities between 74 and 89 km s<sup>-1</sup> (component 5 and 6) are not of interstellar origin, and we attribute them to circumstellar and photospheric material.

The velocity found for component 5 of the NaI D complex is equal to the velocity found for molecular lines absorption (C<sub>2</sub> and CN) which strongly suggests that these lines are formed in the same region. In Sect. 4 we have discussed the physical conditions of the molecular line forming region and found rotational temperatures in agreement with a circumstellar origin. We are now able to conclude that the NaI D component 5 and the C<sub>2</sub> and CN molecular absorption lines are from circumstellar origin. The photospheric contribution is estimated using the standard star  $\alpha$  Per (F5I). This star has NaI D1 and D2 equivalent width of 540 and 500 mÅ. The NaI D component 6 has an equivalent width of the same order, and we argue that this component is photospheric.

## 6. Discussion

The primary aim of this study is to make a line identification of the molecular bands found in the optical spectrum of HD 56126 and to identify the line-forming region. By looking at the absorption components in the NaI D1 and D2 lines and a simple model for the Galactic rotation curve, we are able to separate the NaI D1 and D2 interstellar component (1, 2, 3, and 4) from the circumstellar component (5, C<sub>2</sub>, and CN). The rotational temperature of super-thermal C<sub>2</sub> is  $T_{\text{rot}} = 242 \pm 20$  K, while for sub-thermal CN we find  $T_{\text{rot}} = 24 \pm 5$  K.

In the post-AGB phase the main constituent of the circumstellar material is the last mass-loss episode the star suffered on the AGB. A small contribution of the circumstellar matter might be post-AGB mass loss, but because the escape velocity of a post-AGB object is much higher than for an AGB object, the wind velocities are also much higher. The presence of molecular absorption lines at an expansion velocity of  $-8.5 \text{ km s}^{-1}$  is too low to be attributed to post-AGB mass-loss. This means that these molecules are located in the AGB remnant.

In this study we add to the tracers of the AGB remnant, i.e., infrared energy distribution and millimeter line emission (e.g., CO) a new one: molecular absorption lines. Combining information from different tracers allows us to derive time scales and mass-loss rates. Table 11 gives an overview of the information on the AGB remnant derived from infrared, millimeter, and optical data. Furthermore, we predict the presence of H<sub>2</sub> (e.g., 1108 Å), C<sub>2</sub> (e.g., 1341 Å), and CO (e.g., 1509 Å) in the UV.

Due to self-shielding, CO is not easily photo-dissociated by the UV radiation field and therefore is present out to a large distance from the star in the circumstellar environment. This is not the case for C<sub>2</sub> and CN, as they are much more easily photo-dissociated by the UV radiation field ( $\lambda \leq 2000$  Å). The circumstellar layer where C<sub>2</sub> and CN are present is determined by an interplay between the stellar and interstellar UV radiation field and the local particle density. This implies that CO is detected over the whole AGB remnant, while C<sub>2</sub> and CN are formed over a limited distance range. Furthermore, the millimeter CO emission lines are biased to line-forming regions with a large volume (large distance from the star), while absorption lines are biased to high densities (close to the star). The infrared excess is biased to dust with high temperatures, and thus also to material close to the star. As a first approximation to derive time scales and mass-loss rates from the detection of molecular absorption lines we will assume that the molecular absorption lines originate between the dust inner and outer radius.

We have fitted an optically thin dust model (Waters *et al.* 1988) to the spectral energy distribution (Fig. 7). The best fit was reached for a detached dust shell with a dust inner radius of  $r_1 = 2 \times 10^3 R_*$  ( $= 7 \times 10^{15}$  cm), a dust outer radius of  $r_2 = 8 \times 10^3 R_*$ , and a dust temperature of  $T_{\text{dust}} = 190 - 110$  K. This dust inner radius is in agreement with the work by Hrivnak *et al.* (1989). To calculate the AGB mass-loss rate from the IR, an estimate of the reddening is needed. Here we discuss two approaches to estimate the reddening: (i) from the observed  $(B - V)$  and the intrinsic  $(B - V)_0$  we compute  $E(B - V) = 0.60$  (Table 1). Normalizing the model on the observed energy distribution in the near-infrared, we find that the model strongly underestimated the observed flux near the Balmer jump and argue that  $E(B - V) = 0.60$  cannot explain the observations. (ii) for a spherically symmetric dust shell the energy radiated in the infrared is provided by circumstellar reddening of starlight. We have dereddened the stellar energy distribution and found that the infrared energy output is supported by a circumstellar reddening of  $E(B - V) = 0.40$ . The corresponding model (Fig. 7) is in reasonable agreement with the observations and yields a mass-loss rate of  $\dot{M}_{\text{IR}} = 4 \times 10^{-5} M_{\odot} \text{ yr}^{-1}$ . This is about a factor eight higher than derived by Hrivnak *et al.* (1989). This difference in derived mass-loss rate can partly be explained by the differences in grain characteristics, stellar luminosity, and density law adopted in

the two different models. The deficiency of UV flux might indicate the presence of an additional anomalous circumstellar reddening (e.g.,  $\lambda^{-1}$  for  $\lambda \leq 0.4 \mu\text{m}$ ).

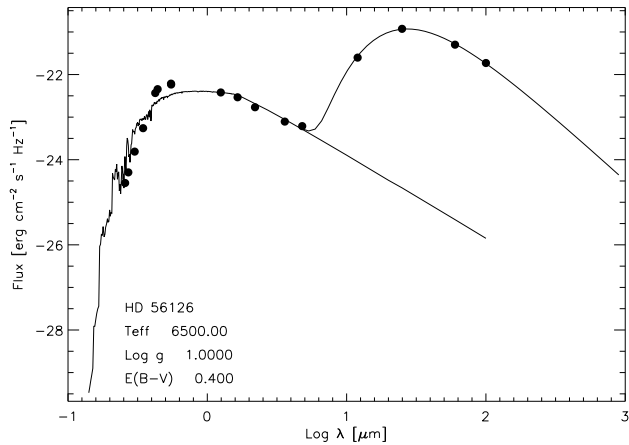


**Fig. 7.** The spectral energy distribution of HD 56126 fitted to a  $T_{\text{eff}} = 6500$  K,  $\log g = 1.0$  Kurucz model and an optically thin dust model. The difference in UV flux between model and observations is probably due to an anomalous circumstellar reddening law.

Combining information from the energy distribution (inner dust radius) and the molecular absorption lines (outflow velocities) makes it possible to calculate the elapsed time since HD 56126 has left the AGB (Eq. 13).

$$t_{\text{left AGB}} = \frac{2.2 \times 10^{-2} \cdot r_1 [R_*]}{v_{\text{exp}} [\text{km s}^{-1}]} = 250 \text{ years} \quad (13)$$

We find that HD 56126 left the AGB about 250 years ago. Such a short time scale is not unusual for post-AGB evolution, as theoretical evolutionary tracks predict transition times from AGB to Planetary Nebula as short as 10,000 years (Schönberner 1983). It is also consistent with the change of spectral type from G5 to F5 in the last 50 years.

$$\dot{M} = 9 \times 10^{-6} \cdot \left( \frac{r_2 r_1 / (r_2 - r_1)}{9.3 \times 10^{15} \text{ cm}} \right) \cdot \left( \frac{v_{\text{exp}}}{8.5 \text{ km s}^{-1}} \right) \cdot \left( \frac{N_{\text{mol}}}{2.0 \times 10^{15} \text{ cm}^{-2}} \right) \cdot \left( \frac{2 \times 10^{-6}}{f_{\text{mol}}} \right) [M_{\odot} \text{ yr}^{-1}] \quad (14)$$

The mass-loss rate from the molecules can be estimated with Eq. 14, with the distance  $r$  in cm,  $v_{\text{exp}}$  in  $\text{km s}^{-1}$ ,  $N_{\text{mol}}$  the column density in  $\text{cm}^{-2}$  (C<sub>2</sub>:  $N_{\text{mol}} = N_{\text{obs}}$  (3,0); CN:  $N_{\text{mol}} = N_{\text{Boltz}}$  (3,0)), and  $f_{\text{mol}}$  the molecular abundance relative to H<sub>2</sub>. We assume that the molecular absorption lines are formed between the dust inner radius ( $r_1 = 2 \times 10^3 R_*$ ) and dust outer radius ( $r_2 = 8 \times 10^3 R_*$ ). Peak abundances of  $f_{\text{C}_2} = f_{\text{CN}} =$

**Table 11.** An overview of the observational tracers of the AGB remnant. A distance of 1.3 kpc derived for an 0.565 M<sub>⊙</sub> post-AGB model (R<sub>\*</sub> = 50 R<sub>⊙</sub>, T<sub>eff</sub> = 6500 K, log L = 3.57 L<sub>⊙</sub>), and log g = 0.5 has been assumed in this table.

Origin	Parameters	$v_{\text{exp}}$ [km s <sup>-1</sup> ]	Ref.
Dust	$T_{\text{dust}} = 110 - 190$ K		1
	$r_1 = 2 \times 10^3$ R <sub>*</sub>		1
	$r_2 = 8 \times 10^3$ R <sub>*</sub>		1
	$\log \dot{M}_{\text{IR}} = -4.4 \pm 1.0$ M <sub>⊙</sub> yr <sup>-1</sup>		1
	$r_1 = 1.4 \times 10^3$ R <sub>*</sub>		2
	$\log \dot{M}_{\text{IR}} = -5.3 \pm 1.0$ M <sub>⊙</sub> yr <sup>-1</sup>		2
<sup>12</sup> CO(J = 1 - 0)	$v = 84.5 \pm 0.5$ km s <sup>-1</sup>	-12.0 ± 1.0	3
<sup>12</sup> CO(J = 2 - 1)	$v = 87 \pm 0.5$ km s <sup>-1</sup>		4
<sup>12</sup> CO(J = 1 - 0)	$v = 86 \pm 0.5$ km s <sup>-1</sup>		4
<sup>13</sup> CO(J = 2 - 1)	$v = 85 \pm 0.5$ km s <sup>-1</sup>		4
<sup>12</sup> CO(J = 1 - 0)	$v = 85.5 \pm 1.0$ km s <sup>-1</sup>	-10.0 ± 2.0	5
Average	$v_{*\text{CO}} = 85.6 \pm 0.5$ km s <sup>-1</sup>		1
	$\log \dot{M}_{\text{CO}} = -4.92 \pm 0.10$ M <sub>⊙</sub> yr <sup>-1</sup>		6
C <sub>2</sub>	$T_{\text{rot}} = 242 \pm 20$ K		1
	$\log N(\text{C}_2) = 15.3 \pm 0.3$ cm <sup>-2</sup>		1
CN	$T_{\text{rot}} = 24 \pm 5$ K		1
	$\log N(\text{CN}) = 15.5 \pm 0.3$ cm <sup>-2</sup>		1
C <sub>2</sub> and CN	$v = 77.1 \pm 0.3$ km s <sup>-1</sup>	-8.5 ± 0.6	1
NaI D1 and D2	$\log \dot{M}_{\text{mol}} = -5 \pm 1$ M <sub>⊙</sub> yr <sup>-1</sup>		1
	$v_{\text{NaI D}} = 75 \pm 2$ km s <sup>-1</sup>	-11 ± 2	1

1: this study; 2: Hrivnak *et al.* 1989; 3: Nyman *et al.* 1992; 4: Bujarrabal *et al.* 1992; 5: Zuckerman *et al.* 1986; 6: Omont *et al.* 1993

$2 \times 10^{-6}$  are taken from the work by Cherchneff and Glassgold (1993) in which they model the carbon-rich circumstellar envelope of IRC+10216. The mass-loss rates found are  $\dot{M}_{\text{C}_2} = 9 \times 10^{-6}$  M<sub>⊙</sub> yr<sup>-1</sup> and  $\dot{M}_{\text{CN}} = 14 \times 10^{-6}$  M<sub>⊙</sub> yr<sup>-1</sup>, and we will adopt a mass-loss rate of  $\dot{M}_{\text{mol}} = 1 \times 10^{-5}$  M<sub>⊙</sub> yr<sup>-1</sup> from the molecular absorption lines with an estimated error of one order. With the above calculation (Eq. 14) we want above all to show that the detection of molecular lines absorption allows the determination of the AGB mass-loss rate. But at this stage the uncertainties in the calculation due to the molecular abundances and the exact distance of the line-forming region to the central star lead to a rather large uncertainty in the value for the derived mass-loss rate. Proper chemical models are required to solve this problem.

An independent technique to determine the mass-loss rate is modeling the population distribution over  $J''$  levels of the electronic-vibrational ground level of C<sub>2</sub> (Bakker *et al.* 1995; Van Dishoeck and Black 1982). This allows the determination of the number of collisional partners (H and H<sub>2</sub>) and hence the AGB mass-loss rate. This work is still in progress and will be published in a separate paper.

The problem of a change of mass-loss rate along the AGB can only be studied if there are tracers available which are formed in different regions of the AGB remnant. The observed millimeter CO emission is at larger distance

from the star than the C<sub>2</sub> and CN molecular lines. Comparing the expansion velocities of the C<sub>2</sub> and CN absorption lines with the CO expansion velocities tells us whether there is a change in expansion velocity of the AGB wind during the last episode of the AGB phase. As CO has an expansion velocity of  $-10 \pm 2$  km s<sup>-1</sup> whereas C<sub>2</sub> and CN have an expansion velocity of  $-8.5 \pm 0.6$  km s<sup>-1</sup>, the difference between those velocities of 2.6 km s<sup>-1</sup> is only a 2σ deviation, and we are not able to show whether or not the expansion velocity of the AGB wind has changed as the star evolved along the AGB.

## 7. Conclusion

We have identified molecular line absorption in the optical spectrum of the post-AGB star HD 56126 of C<sub>2</sub> (Phillips (1,0), (2,0), and (3,0); Swan (1,0) and (0,0)), and CN (Red system (1,0), (2,0), (3,0), and (4,0)). For all molecular lines we find the same expansion velocity relative to the CO millimeter line emission of  $-8.5 \pm 0.6$  km s<sup>-1</sup> and identify the line-forming region in the AGB remnant. We find that the C<sub>2</sub> molecular lines in the (1,0) and (2,0) Phillips band are optically thick, whereas the Phillips (3,0) band is optically thin. For the C<sub>2</sub> Phillips (3,0) we find a rotational temperature of  $T_{\text{rot}} = 242 \pm 20$  K and a column density of  $N_{\text{Boltz}} = 2.0 \times 10^{15}$  cm<sup>-2</sup>. For the CN Red system (3,0) we find  $T_{\text{rot}} = 24 \pm 5$  K and  $N_{\text{Boltz}} = 3.3 \times 10^{15}$  cm<sup>-2</sup>. Assum-

ing that the molecular absorption lines are formed at the dust inner radius and the molecular abundances are equal to those in the circumstellar envelope of IRC+10216, we find a mass-loss rate of  $\dot{M}_{\text{mol}} = 1 \times 10^{-5} M_{\odot} \text{ yr}^{-1}$  with an estimated error of one order.

We have started a systematic survey of molecular absorption and emission lines in the optical spectra of post-AGB stars in order to fully exploit this new approach to study the AGB remnant.

*Acknowledgements.* This work would not have been possible without the contribution of Ton Schoenmaker and Ewine van Dishoeck. In reducing the raw data to handsome spectra Ton provides us with the data to do this study whereas Ewine has introduced us in the field of molecular spectroscopy and astrochemistry. The authors want to thank Christoffel Waelkens, René Oudmaijer, and Hans van Winckel for the stimulating and constructive discussions on this work. The referee, Prof. A. Omont, has made a valuable contribution by suggesting important changes to this article. EJB was supported by grant no. 782-371-040 by ASTRON, which receives funds from the Netherlands Organization for the Advancement of Pure Research (NWO). LBFMW is supported by the Royal Netherlands Academy of Arts and Sciences. This research has made use of the Simbad database, operated at CDS, Strasbourg, France.

## References

- Amiot C.: 1983, *ApJS* 52, 329
- Bakker E.J., Lamers H.J.G.L.M., Waters L.B.F.M., Schoenmaker S.: 1995, *Ap.Sp.Sci* 224, 335, in: "Circumstellar matter", eds. G.D. Watt and P.M. Williams
- Barnbaum C.: 1994, *ApJS* 90, 317
- Ballik E.A., Ramsay D.A.: 1976, *J.Mol.Spectr.* 84, 120
- Bergeat J., Sibille F., Lunel M., Lefevre J.: 1976, *A&A* 52, 227
- Bujarrabal V., Alcolea J., Planesas P.: 1992, *A&A* 257, 701
- Chauville J., Maillard J.P., Mantz A.W.: 1977, *J.Mol.Spectr.* 68, 399
- Cherchneff I., Glassgold A.E.: 1993, *ApJ* 419, L41
- Cherchneff I., Glassgold A.E., Mamon G.A.: 1993, *ApJ* 410, 188
- Davis S. P., Shortenhaus D., Stark G., Engleman R., Phillips J.G., Hubbard R.P.: 1986, *ApJ* 303, 892
- Dinerstein H.L., Sneden C., Uglum J.: 1995, *ApJ*, in press
- Draine B.T.: 1978, *ApJS* 36, 595
- Dunham, T.Jr.: 1941, *Pub.A.A.S.* 10, 123
- Herzberg G.: 1950, "Molecular Spectra and Molecular Structure, I. Spectra of Diatomic Molecules", second edition
- Hrivnak B.J., Kwok S., Volk K.M.: 1989, *ApJ* 346, 265
- Hrivnak B.J.: 1995, *ApJ* 438, 341
- Iben I.Jr.: 1983, *ARAA* 21, 271
- IRAS catalogue, volume 1-6, *Explanatory Supplement and Point Source Catalogue*, Joint IRAS Science Work Group: 1986, NASA RP-1190
- Jørgenson U.G., Larson M.: 1990, *A&A* 238, 424
- Klochkova V.G.: 1995, *MNRAS* 272, 710
- Kwok S., Volk K., Hrivnak B.J.: 1989, *ApJ* 345, L51
- Lang K.R.: 1980, "Astrophysical Formulae", second edition, Springer-Verlag
- Nassau J.J., Stephenson C.B., MacConnell D.J.: 1965, *Luminous stars in the Northern Milky Way VI* (Hamburg: Hamburg Sternwarte and Warner and Swasey observatory)
- Moore Ch.E.: Feb. 1972, A multiplet table of astrophysical interest, *Nat. Stand. Ref. Data. Ser. Bur. Stand.* 40
- Moore Ch.E., Minnaert M.G.J., Houtgast J.: 1966, *The Solar Spectrum 2935 Å to 8770 Å*, NBS Mono. 61
- Nyman L.Å., Booth R.S., Carlström U., Habing H.J., Heske A., Sahai R., Stark R., Van der Veen W.E.C.J., Winnberg A.: 1992, *A&AS* 93, 121
- Omont A., Loup C., Forveille T., Te Lintel Hekkert P., Habing H., Sivagnanam P.: 1993, *A&A* 267, 515
- Oudmaijer R.D., Van der Veen W.E.C.J., Waters L.B.F.M., Trams N.R., Waelkens C., Engelsman E.: 1992, *A&AS* 96, 625
- Oudmayer R.D., Bakker E.J.: 1994, *MNRAS* 271, 615
- Parthasarathy M., Pottasch S.R.: 1986, *A&A* 154, L16
- Parthasarathy M., Garcia-Lario P., Pottasch S.R.: 1992, *A&A* 264, 159
- Schönberner D.: 1983, *ApJ* 272, 708
- Souza S.P., Lutz B.L.: 1977, *ApJ* 216, L49, erratum 218, L31
- Trams N.R., Waters L.B.F.M., Lamers H.J.G.L.M., Waelkens C., Geballe T.R., Thé P.S.: 1991, *A&AS* 87, 361
- Van Dishoeck E.F.: 1983, *Chem.Phys.* 77, 277
- Van Dishoeck E.F., De Zeeuw T.: 1984, *MNRAS* 206, 383
- Van Dishoeck E.F., Black J.H.: 1982, *ApJ* 258, 533
- Wallace L.: 1962, *ApJS* 68, 165
- Waters L.B.F.M., Coté J., Geballe T.R.: 1988, *A&A* 203, 348
- Whiting E.E.: 1973, *NASA TN D-7268*
- Zuckerman B., Dyck H.M., Claussen M.J.: 1986, *ApJ* 304, 401

## A. Molecular lines identification of C<sub>2</sub> and CN

We present a complete line identification of the C<sub>2</sub> Phillips bands (1,0), (2,0), and (3,0), and the CN Red system (1,0) and (2,0). Each table (only available at CDS) gives for a rotational band the line identification (column 1) and the laboratory wavelength (column 2) in **air**. The wavelength conversion from vacuum to air was made by applying Cauchy's formula. The data on the laboratory wavelength and the oscillator strength were obtained from a variety of sources. Most of the references are given in Table 7. The observational parameters of the rotational line identified are given in columns 3 and 4, the observed wavelength and the observed equivalent width (mÅ) respectively. From these values the column densities can be calculated under the assumption of optically thin lines. The conversion from equivalent width to column density is explained in Sect. 4. The last column gives a remark if applicable. It should be noted that we do not have a complete wavelength coverage in the wavelength interval observed. For longer wavelength than 6030 Å the echellogram is larger in the dispersion direction than the size of the CCD. This results in gaps between two successive orders in the spectrum. The data of CN has been taken from Jørgenson and Jarson (1990).

## B. Photospheric CI, NI, and OI lines

The heliocentric velocity of the star have been obtained by an accurate Gaussian fit to high-excitation CI, NI, and OI lines. The table gives a list of identified lines and the observational parameters. This table has the same layout as the tables pre-

sented in App. A. For a description of the table we refer to the introduction of App. A. The atomic data is taken from Moore (1972).

**Table 12.** Line identification list of photospheric Cl, NI, and OI

$\lambda_{\text{lab}}$ [Å]	Atom (mtp)	$\chi$ [eV]	$\lambda_{\text{obs}}$ [Å]	$W_{\lambda}$ [mÅ]	$D$ %	$v_{\odot}$ [km/s]
9078.32	Cl(3)	7.45	9081.4	626.8	0.74	80
9061.48	Cl(3)	7.45	9064.6	525.5	0.58	82
9062.53	Cl(3)	7.45	9065.5	683.4	0.62	80
8242.34	NI(2)	10.29	8245.2	59.2	0.13	83
7771.96	OI(1)	9.11	7774.7	570.6	0.59	84
7774.18	OI(1)	9.11	7776.9	544.8	0.59	84
7775.40	OI(1)	9.11	7778.1	474.9	0.56	83



**Table 13.** Identification of the (1,0) band in the C<sub>2</sub> A<sup>1</sup>Π<sub>u</sub> – X<sup>1</sup>Σ<sub>g</sub><sup>+</sup> Phillips system

Branch ( $J''$ )	$\lambda_{\text{lab}}$ [Å]	$\lambda_{\text{obs}}$ [Å]	$W_{\lambda}$ [mÅ]	$f_{J'J''} 10^4$	$N_{J''}$ [10 <sup>12</sup> cm <sup>-2</sup> ]	Remark
R( 0)	10143.726	10147.18	43.2	28.41	16.7	blend on red wing
P( 2)	10154.900	10158.42	32.2	2.84	124.2	
Q( 2)	10148.354	10151.89	37.2	14.20	28.7	
R( 2)	10138.542	10141.97	35.5	11.36	342.3	
P( 4)	10164.764	10168.22	47.5	4.72	110.1	cosmic hit
Q( 4)	10151.525	10154.99	38.9	14.19	30.1	cosmic hit
R( 4)	10135.151	10138.61	60.5	9.48	70.2	
P( 6)	10176.254	10179.81	32.4	5.45	64.9	
Q( 6)	10156.518	10160.05	39.4	14.18	30.4	
R( 6)	10133.605	10137.21	87.3	8.75		blended with R( 8)
P( 8)	10189.695			5.82		≤14 Å
Q( 8)	10163.326	10166.89	44.5	14.18	34.3	
R( 8)	10133.857	10137.21	87.3	8.36		blended with R( 6)
P(10)	10205.000	10208.57	45.8	3.56	139.6	
Q(10)	10171.965	10175.57	40.7	14.16	31.4	
R(10)	10135.925	10139.39	29.7	8.12	40.2	
P(12)	10222.174			6.20		not observed
Q(12)	10182.436			14.15		≤15 Å
R(12)	10139.807	10143.33	36.6	7.96	50.5	
P(14)	10241.248			6.31		not observed
Q(14)	10194.757	10198.38	48.6	14.13	18.9	
R(14)	10145.507	10148.98	35.0	7.83	49.1	
P(16)	10262.232			6.38		not observed
Q(16)	10208.933	10212.52	50.5	14.11	38.8	
R(16)	10153.034	10156.60	37.1	7.74	52.5	
P(18)	10285.144			6.44		not observed
Q(18)	10224.985			14.09		not observed
R(18)	10162.400	10166.00	30.3	7.66	43.3	
P(20)	10310.011			6.48		≤15 Å
Q(20)	10242.923			14.07		not observed
R(20)	10173.608	10177.19	29.4	7.60	42.2	
P(22)	10336.863			6.50		≤ 15 Å
Q(22)	10262.768			14.04		not Observed
R(22)	10186.670	10190.27	19.9	7.54	28.7	
P(24)	10365.711			6.52		≤15 Å
Q(24)	10284.541			14.01		not observed
R(24)	10201.603	10205.08	13.5	7.49	19.6	
P(26)	10396.593			6.54		≤ 15 Å
Q(26)	10308.256			13.98		≤ 15 Å
R(26)	10218.418			7.45		≤ 15 Å
P(28)	10429.547			6.54		not observed
Q(28)	10333.947			13.94		not observed
R(28)	10237.138			7.41		not observed
P(30)	10464.598			6.54		not observed
Q(30)	10361.633			13.90		≤ 15 Å
R(30)	10257.781			7.37		not observed

**Table 14.** Identification of the (2,0) band in the C<sub>2</sub> A<sup>1</sup>Π<sub>u</sub> – X<sup>1</sup>Σ<sub>g</sub><sup>+</sup> Phillips system

Branch ( $J''$ )	$\lambda_{\text{lab}}$ [Å]	$\lambda_{\text{obs}}$ [Å]	$W_{\lambda}$ [mÅ]	$f_{J'J''}10^4$	$N_{J''}$ [10 <sup>12</sup> cm <sup>-2</sup> ]	Remark
R( 0)	8757.686	8760.54	33.2	16.70	29.3	
P( 2)	8766.031	8768.90	22.9	1.67	201.6	
Q( 2)	8761.197	8764.08	42.5	8.35	74.9	
R( 2)	8753.949	8756.81	28.4	6.68	44.6	
P( 4)	8773.430	8776.30	34.3	2.78	181.1	
Q( 4)	8763.754	8766.62	50.0	8.35	88.1	
R( 4)	8751.687	8754.40	37.2	5.57		blended with R( 8)
P( 6)	8782.311	8785.18	41.1	3.20	188.2	
Q( 6)	8767.762	8770.61	40.6	8.34	71.6	
R( 6)	8750.850	8753.70	31.3	5.14	52.0	blended with P(12)
P( 8)	8792.652	8795.53	29.1	3.43	124.0	
Q( 8)	8773.223	8776.09	36.9	8.34	65.0	
R( 8)	8751.490	8754.40	37.2	4.92		blended with R( 4)
P(10)	8804.502	8807.37	26.5	3.56	108.5	
Q(10)	8780.144	8783.04	37.0	8.33	65.2	
R(10)	8753.581	8756.43	25.7	4.77	45.1	
P(12)	8817.830			3.65		not observed
Q(12)	8788.561	8791.44	36.7	8.32	64.5	
R(12)	8757.130	8759.99	32.0	4.68	100.8	
P(14)	8832.682			3.71		not observed
Q(14)	8798.462	8801.34	30.4	8.31	53.4	
R(14)	8762.147	8765.04	25.6	4.61	81.7	
P(16)	8849.075			3.76		not observed
Q(16)	8809.844			8.30		not observed
R(16)	8768.631	8771.52	17.3	4.55	55.9	
P(18)	8866.997			3.79		not observed
Q(18)	8822.728			8.29		not observed
R(18)	8776.611	8779.49	14.0	4.50	29.7	
P(20)	8886.487	8889.43	14.7	3.81	55.2	
Q(20)	8837.122			8.28		not observed
R(20)	8786.050	8788.94	12.0	4.47	24.7	
P(22)	8907.545	8910.47	6.9	3.83	25.7	
Q(22)	8853.044	8855.96	11.0	8.26	19.2	
R(22)	8796.979	8799.85		4.43	54.7	tentatively detected ≤ 5 Å
P(24)	8930.172			3.84		
Q(24)	8870.519	8873.38	11.7	8.24	20.4	
R(24)	8809.410			4.41		not observed
P(26)	8954.440			3.85		not observed
Q(26)	8889.535	8892.43	10.8	8.23		tentative detection
R(26)	8823.379			4.38		not observed
P(28)	8980.336			3.86		not observed
Q(28)	8910.135	8913.09	5.1	8.21		tentative detection
R(28)	8838.846			4.36		not observed
P(30)	9007.897			3.86		≤ 5 Å
Q(30)	8932.333			8.19		≤ 5 Å
R(30)	8855.876			4.33		≤ 5 Å

**Table 15.** Identification of the (3,0) band in the C<sub>2</sub> A<sup>1</sup>Π<sub>u</sub> – X<sup>1</sup>Σ<sub>g</sub><sup>+</sup> Phillips system

Branch ( $J''$ )	$\lambda_{\text{lab}}$ [Å]	$\lambda_{\text{obs}}$ [Å]	$W_{\lambda}$ [mÅ]	$f_{J'J''} 10^4$	$N_{J''}$ [10 <sup>12</sup> cm <sup>-2</sup> ]	Remark
R( 0)	7719.331	7721.87	30.5	7.52	76.9	
P( 2)	7725.822	7728.37	16.4	0.75	414.0	
Q( 2)	7722.096	7724.62	34.7	3.76	174.9	
R( 2)	7716.531	7719.05	29.5	3.01	186.0	
P( 4)	7731.666	7734.21	29.2	1.25	441.6	
Q( 4)	7724.222	7726.76	35.6	3.76		telluric pollution
R( 4)	7714.947	7717.48	30.7	2.51	232.2	
P( 6)	7738.740	7741.28	20.6	1.44	269.9	
Q( 6)	7727.560	7730.12	37.9	3.76		telluric pollution
R( 6)	7714.578	7717.12	28.0	2.32	229.2	
P( 8)	7747.040			1.54		not observed
Q( 8)	7732.120	7734.66	29.6	3.75	149.2	
R( 8)	7715.418	7717.94	24.0	2.21	206.1	
P(10)	7756.585			1.60		not observed
Q(10)	7737.908	7740.43	27.9	3.75		blended with R(18)
R(10)	7717.473	7720.00	14.2	2.15	125.3	
P(12)	7767.372	7769.89	13.7	1.64	156.5	
Q(12)	7744.903			3.75		not observed
R(12)	7720.751	7723.28	23.1	2.11	207.5	
P(14)	7779.431	7781.95	14.0	1.67	156.5	
Q(14)	7753.144			3.74		not observed
R(14)	7725.243	7727.74	13.1	2.07		telluric pollution
P(16)	7792.741	7795.24	6.4	1.69		tentative detection
Q(16)	7762.626			3.74		not observed
R(16)	7730.966	7733.51	11.4	2.05	105.1	
P(18)	7807.322	7809.86	3.0	1.71		tentative detection
Q(18)	7773.358	7775.92	7.9	3.73		blended with OI(1)
R(18)	7737.908	7740.43	27.9	2.03		blended with Q(10)
P(20)	7823.201			1.72		≤ 5 Å
Q(20)	7785.350	7787.85	11.5	3.73		telluric pollution
R(20)	7746.098			2.01		not Observed
P(22)	7840.387			1.73		pollution
Q(22)	7798.613			3.72		telluric pollution
R(22)	7755.532			2.00		not observed
P(24)	7858.889			1.73		not observed
Q(24)	7813.138			3.72		≤ 5 Å
R(24)	7766.226			1.98		≤ 5 Å
P(26)	7878.721			1.74		pollution
Q(26)	7828.979			3.71		≤ 5 Å
R(26)	7778.178			1.97		≤ 5 Å
P(28)	7899.907			1.74		≤ 5 Å
Q(28)	7846.122			3.70		not observed
R(28)	7791.405			1.96		≤ 5 Å
P(30)	7922.464			1.74		≤ 5 Å
Q(30)	7864.595			3.69		not observed
R(30)	7805.908			1.95		≤ 5 Å

**Table 16.** Identification of the (1,0) band of the CN A<sup>2</sup>Π – X<sup>2</sup>Σ<sup>-</sup> transition

Transition	$J''$	$N''$	$\lambda_{\text{lab}}$ [Å]	$\lambda_{\text{obs}}$ [Å]	$W_{\lambda}$ [mÅ]	$f_{J',J''} 10^4$	$N_{N'',J''}$ [10 <sup>12</sup> cm <sup>-2</sup> ]	Remark
SR21	3/2	1	9135.582	NO		1.74		
SR12	1/2	0	9139.686	9142.70	33.7	2.54	179.4	
RQ21	7/2	3	9141.189	9144.21	35.3	3.65	130.7	
R2	5/2	3	9141.169	blend		3.43		
RQ21	5/2	2	9141.886	9144.88	57.8	3.99	195.7	
R2	3/2	2	9141.870	blend		3.44		
RQ21	3/2	1	9142.838	9145.82	57.8	6.14	127.2	blended
R2	1/2	1	9142.828	blend		3.65		
RQ21	1/2	0	9144.042	9147.04	57.8	6.14	127.1	
Q2	1/2	1	9147.208	9150.18	61.5	6.14	135.2	
QP12	3/2	1	9147.217	blend		1.55		
Q2	3/2	2	9149.167	9152.19	47.0	5.36	118.3	
QP21	5/2	2	9149.182	blend		1.74		
Q2	5/2	3	9151.381	9154.38	31.1	5.50	76.2	
QP21	7/2	3	9151.401	blend		1.73		
P2	3/2	2	9153.532	9156.62	27.4	1.55	238.2	
R1	7/2	3	9177.032	9180.04	31.5	4.71	89.7	
R1	5/2	2	9179.911	9182.95	47.6	5.16	123.6	
R1	3/2	1	9183.209	9186.24	101.8	6.19	220.2	
R1	1/2	0	9186.932	9189.96	59.9	9.79	81.9	
Q1	7/2	3	9189.486	9192.61	97.8	5.44		blended
Q2	5/2	2	9189.597	blend		4.99		
QR12	5/2	3	9189.465	blend		3.60		
QR12	3/2	2	9189.581	blend		4.87		
QR12	1/2	1	9190.120	9193.18	62.9	8.68	96.9	
Q1	3/2	1	9190.129	blend		4.13		
PQ12	3/2	2	9196.511	9199.58	42.2	3.26	172.8	
P1	5/2	2	9196.525	blend		0.72		
PQ12	5/2	3	9199.171	9202.23	22.2	3.48	85.1	
P1	7/2	3	9199.192	blend		1.24		

**Table 17.** Identification of the (2,0) band of the CN A<sup>2</sup>Π – X<sup>2</sup>Σ<sup>-</sup> transition

Transition	$J''$	$N''$	$\lambda_{\text{lab}}$ [Å]	$\lambda_{\text{obs}}$ [Å]	$W_{\lambda}$ [mÅ]	$f_{J',J''} 10^4$	$N_{N'',J''}$ [10 <sup>12</sup> cm <sup>-2</sup> ]	Remark
SR21	1/2	0	7871.654	7874.2	29.4	1.28		blended
R2	5/2	3	7872.889			1.73		blended
RQ21	7/2	3	7872.905	7875.4	18.5	1.84		blended
R2	3/2	2	7873.332			1.73		blended
RQ21	5/2	2	7873.343	7875.9	38.8	2.02		blended
R2	1/2	1	7873.985			1.84		blended
RQ21	3/2	1	7873.992	7876.5	45.8	2.26		blended
RQ21	1/2	0	7874.852	7877.4	39.1	3.09	230.2	
Q2	1/2	1	7877.198	7879.8	98.2	3.09		polluted
QP21	3/2	1	7877.205			0.78		not detected
Q2	3/2	2	7878.686	7881.2	35.6	2.70	240.0	
QP21	5/2	2	7878.697			0.88		not detected
Q2	5/2	3	7880.384	7882.9	19.2	2.77	126.2	
QP21	7/2	3	7880.400			0.88		not detected
P2	3/2	2	7881.889			0.78		not detected
P2	5/2	3	7885.725			0.98		not detected
R1	7/2	3	7899.481	7901.8	42.0	2.37		pollution
R1	5/2	2	7901.520	7904.1	31.6	2.59	220.8	
R1	3/2	1	7903.892	7906.5	41.3	3.12	239.5	
R1	1/2	0	7906.598	7909.2	46.3	4.93	169.6	
QR12	5/2	3	7908.597			1.81		blended
QR12	3/2	2	7908.611	7911.2	50.1	2.45		blended
Q1	7/2	3	7908.613			2.73		blended
Q1	5/2	2	7908.622			2.50		blended
QR12	1/2	1	7908.959	7911.5	53.3	4.37		blended
Q1	3/2	1	7908.966			2.08		blended
PQ12	3/2	2	7913.692	7916.3	19.1	1.64	210.0	
P1	5/2	2	7913.704			0.36		not detected
PQ12	5/2	3	7915.714	7918.3	18.5	1.75	190.3	
P1	7/2	3	7915.729			0.62		not detected
OP12	5/2	3	7920.804			0.26		not detected

**Table 18.** Identification of the (3,0) band of the CN A<sup>2</sup>Π – X<sup>2</sup>Σ<sup>-</sup> transition

Transition	$J''$	$N''$	$\lambda_{\text{lab}}$ [Å]	$\lambda_{\text{obs}}$ [Å]	$W_{\lambda}$ [mÅ]	$f_{J',J''} 10^4$	$N_{N'',J''}$ [10 <sup>12</sup> cm <sup>-2</sup> ]	Remark
SR21	7/2	3	6918.598			0.3773		
SR21	5/2	2	6920.501			0.4182		
SR21	3/2	1	6922.587	6924.9	30.2	0.4744		weak
SR21	1/2	0	6924.855			0.5612		
R2	5/2	3	6925.917			0.7582		
RQ21	7/2	3	6925.929			0.8108		
R2	3/2	2	6926.197			0.7601		
RQ21	5/2	2	6926.206	6928.5	17.2	0.8840	458.0	
R2	1/2	1	6926.659			0.8061		blended
RQ21	3/2	1	6926.665	6928.9	21.6	0.9896		blended
RQ21	1/2	0	6927.302	6929.6	27.1	1.3570	469.9	
Q2	1/2	1	6929.119	6931.4	18.9	1.3570	327.6	
QP21	3/2	1	6929.124			0.3418		
Q2	3/2	2	6930.297	6932.6	12.9	1.1835	256.3	
QP21	5/2	2	6930.305			0.3842		
Q2	5/2	3	6931.655			1.2138		
QP21	7/2	3	6931.667			0.3850		
P2	3/2	2	6932.748			0.3418		
P2	5/2	3	6935.742			0.4318		
R1	7/2	3	6946.486			1.0377		
R1	5/2	2	6947.992	6950.3	14.3	1.1356	294.6	
R1	3/2	1	6949.770	6952.1	24.0	1.3620	412.0	
R1	1/2	0	6951.821	6954.1	34.1	2.1529	370.1	
QR12	3/2	2	6953.418			1.0763		blended
Q1	5/2	2	6953.427			1.0982		blended
QR12	5/2	3	6953.462			0.7990		blended
Q1	7/2	3	6953.475			1.1983		blended
QR12	1/2	1	6953.646	6955.9	52.8	1.9182		blended
Q1	3/2	1	6953.652			0.9131		blended
PQ12	3/2	2	6957.305	6959.6	7.9	0.7193	256.2	
P1	5/2	2	6957.314			0.1598		
PQ12	5/2	3	6958.908	6961.2	12.8	0.7684	388.4	
P1	7/2	3	6958.920			0.2703		
OP12	5/2	3	6962.801			0.1122		